UNCLASSIFIED

SECURITY CLASSIFICATION OF THIS PAGE *(When Data Entered)*

REPORT DOCUMENTATION PAGE		READ INSTRUCTIONS BEFORE COMPLETING FORM
1. REPORT NUMBER	2. GOVT ACCESSION NO.	3. RECIPIENT'S CATALOG NUMBER
4. TITLE *(and Subtitle)* ACOUSTIC MICROSCOPY AT CRYOGENIC TEMPERATURES		5. TYPE OF REPORT & PERIOD COVERED Final Report July 1 1977-June 30 1984 6. PERFORMING ORG. REPORT NUMBER G.L. Report No. 3795
7. AUTHOR(s) Daniel Rugar John Foster C. F. Quate		8. CONTRACT OR GRANT NUMBER(s) N00014-77-C-0412
9. PERFORMING ORGANIZATION NAME AND ADDRESS Edward L. Ginzton Laboratory Stanford University Stanford, California 94305		10. PROGRAM ELEMENT, PROJECT, TASK AREA & WORK UNIT NUMBERS Program Element No. 61153N Project-Task Area No. RR011-08-01 Work Unit No. NR 384-924
11. CONTROLLING OFFICE NAME AND ADDRESS Office of Naval Research Physics Division Office (Code 412) Arlington, Virginia 22217		12. REPORT DATE November 1984 13. NUMBER OF PAGES 99
14. MONITORING AGENCY NAME & ADDRESS*(if different from Controlling Office)*		15. SECURITY CLASS. *(of this report)* UNCLASSIFIED 15a. DECLASSIFICATION/DOWNGRADING SCHEDULE

16. DISTRIBUTION STATEMENT *(of this Report)*

Approved for public release; distribution unlimited.

17. DISTRIBUTION STATEMENT *(of the abstract entered in Block 20, if different from Report)*

18. SUPPLEMENTARY NOTES

19. KEY WORDS *(Continue on reverse side if necessary and identify by block number)*

Cryogenic Acoustic Microscope
Superfluid helium
Nonlinear acoustics
Sound attenuation
Sound scattering

20. ABSTRACT *(Continue on reverse side if necessary and identify by block number)*

The resolution of the acoustic microscope is greatly enhanced by using cryogenic liquids for the coupling medium. Liquid Argon, Nitrogen, and Superfluid Helium have all been used for acoustic microscopy during this program. Superfluid helium at temperatures less than 0.2 K emerges as the ultimate fluid for high resolution acoustic microscopy. Using coherent 300 Å sound waves in helium, images with a resolution of 200 Å have been produced.

DD FORM 1 JAN 73 1473 EDITION OF 1 NOV 65 IS OBSOLETE
S/N 0102-LF-014-6601

UNCLASSIFIED

SECURITY CLASSIFICATION OF THIS PAGE *(When Data Entered)*

Edward L. Ginzton Laboratory
W.W. Hansen Laboratories of Physics
Stanford University
Stanford, California

ACOUSTIC MICROSCOPY AT CRYOGENIC TEMPERATURES

Final Report

for the period

July 1, 1977 - June 30, 1984

Contract No. N00014-77-C-0412

Principal Investigator: Professor C. F. Quate

G.L. Report No. 3795

November 1984

W.W. HANSEN LABORATORIES OF PHYSICS
STANFORD UNIVERSITY
STANFORD, CALIFORNIA 94305-2184

Edward L. Ginzton Laboratory
High Energy Physics Laboratory

Telephone (415) 497- 0213

December 6, 1984

Office of Naval Research
Physics Division Office (Code 412)
800 North Quincy Street
Arlington, Virginia 22217

Dear Sir:

Enclosed please find two copies of our Final Report under Contract No. N00014-77-C-0412 for the research program entitled "Acoustic Microscopy at Cryogenic Temperatures". This report covers the period July 1, 1977 to June 30, 1984.

Distribution has been made in accordance with the ONR Physics Division Office Distribution List dated April 1984.

Sincerely,

C. F. Quate
Professor of Applied Physics
and Electrical Engineering
Principal Investigator

CFQ:am
Encls: Final Report (G.L. Report No. 3795)
c.c. R. A. Simpson, ONR Resident Representative, SU
G.L. Reports Office

TABLE OF CONTENTS

TABLE OF CONTENTS (Continued)

1. INTRODUCTION

The Scanning Acoustic Microscope was introduced by C.F. Quate and R.A. Lemons in 1973.[1] The first microscope used water as the coupling fluid between the acoustic lens and the sample. After ten years of research, the water acoustic microscope now features resolution comparable to the very best optical microscopes[2] (< 2000 Å). It is capable of measuring elastic and subsurface properties of materials. Other liquids besides water, however, may be used for acoustic microscopy, and for high resolution we shall see that low temperature superfluid helium emerges as the "ultimate" fluid for acoustic imaging.[3] The principle advantage of the low temperature helium is its extremely small acoustic attenuation. Helium has the additional advantage of a very low sound velocity. This report will describe the successful construction and use of the superfluid helium acoustic microscope operating at temperatures less than 0.1 K. This microscope now offers a lateral resolution of 200 Å and unique contrast mechanisms which have provided sample images showing structures never seen before.[3,4]

A. THE ACOUSTIC MICROSCOPE

Figure 1.1 shows the general schematic and principles of the acoustic microscope. The heart of the microscope is the lens which is typically made from sapphire ($A\ell_2O_3$). A spherical depression is polished at one end of the sapphire, and the other end is polished flat. A thin film ZnO transducer is deposited on the flat end, and a

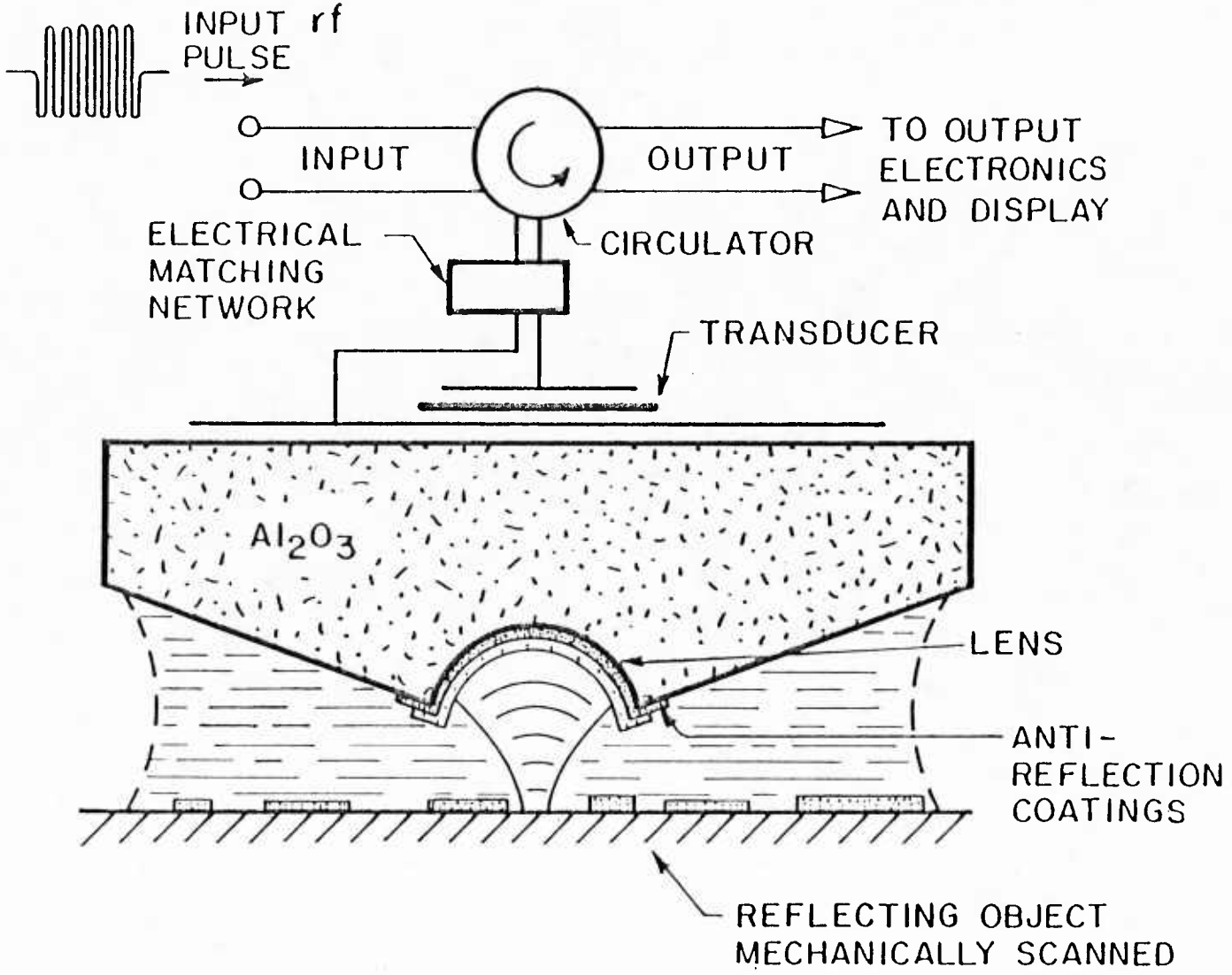

FIGURE 1.1--Configuration of the reflection acoustic microscope.

quarter-wave thick acoustic impedance matching layer is deposited on the spherical depression.[5] The lens is placed near the sample with a liquid coupling between them, as shown in Fig. 1.1. If a pulse of microwave radiation is applied to the transducer, plane longitudinal sound waves are generated and propagate down the sapphire rod. Since liquid sound speeds are typically much less than sound speeds in solids, the acoustic plane waves refract across the spherical interface and come to a tight focus in the liquid. If the sample is placed near the focus, part of the acoustic radiation will reflect from the surface, return to the lens, and again become plane waves in the sapphire. This signal can be received with the transducer and the intensity of the "echo" from the surface is recorded. To form an image, the microwaves are repeatedly pulsed while the lens is mechanically scanned across the sample. The echo intensity is recorded as a function of position, and the result is displayed directly on a CRT.

To achieve the low temperature of operation, the superfluid helium acoustic microscope is cooled using a ^3He-^4He dilution refrigerator. Figure 1.2 shows the acoustic scanning assembly designed for the microscope.[6] This assembly is bolted to the mixing chamber of the refrigerator, and filled with enough helium, approximately 30 ml, to fully immerse the lens and mechanical scanner. The sample to be examined by the microscope is mounted on a 7 foot focusing rod which extends to room temperature. A coarse adjustment of microscope focus is achieved using a room temperature differential micrometer connected to the sample holding rod. Fine focusing is achieved by adjusting the

voltage to a piezoelectric positioning element consisting of a 2.5 cm long PZT-5H tube.

The mechanical scanner shown in Figure 1.2 moves the acoustic lens while the sample is fixed. The acoustic lens is mounted on the end of a 10 cm long section of stainless steel semi-rigid coaxial cable. The coaxial cable serves both as the carrier of microwave signals to and from the acoustic lens, and as a flexible, spring-like support for the lens; when a picture is taken, the lens is translated electro-mechanically in a two-dimensional rastor pattern by means of orthogonally mounted drive coils. The transverse scanning velocity of the lens is sensed by two additional coils; only one pair of drive and sense coils is shown in Figure 1.2. The velocity signals from the sense coils are electronically integrated to obtain information on the position of the lens. The accuracy with this simple scanning system is better than 200 Å.

The resolution of the acoustic microscope is determined by the focal spot size. The spot size in all of the experiments reported here is diffraction limited, and the resolution[7] is approximately equal to $F\lambda$, where F is the F-number of the lens (aperture diameter divided by focal length) and λ is the acoustic wavelength in the liquid. Since $\lambda = c/f$ where c is the sound speed and f is the frequency, the resolution is improved by using liquids with low sound speeds and by increasing the frequency. A fundamental limitation occurs, however, when the acoustic attenuation in the liquid path becomes so large that the signal-to-noise ratio is unacceptable. The acoustic attenuation is important because the input signal is limited in the linear case (see

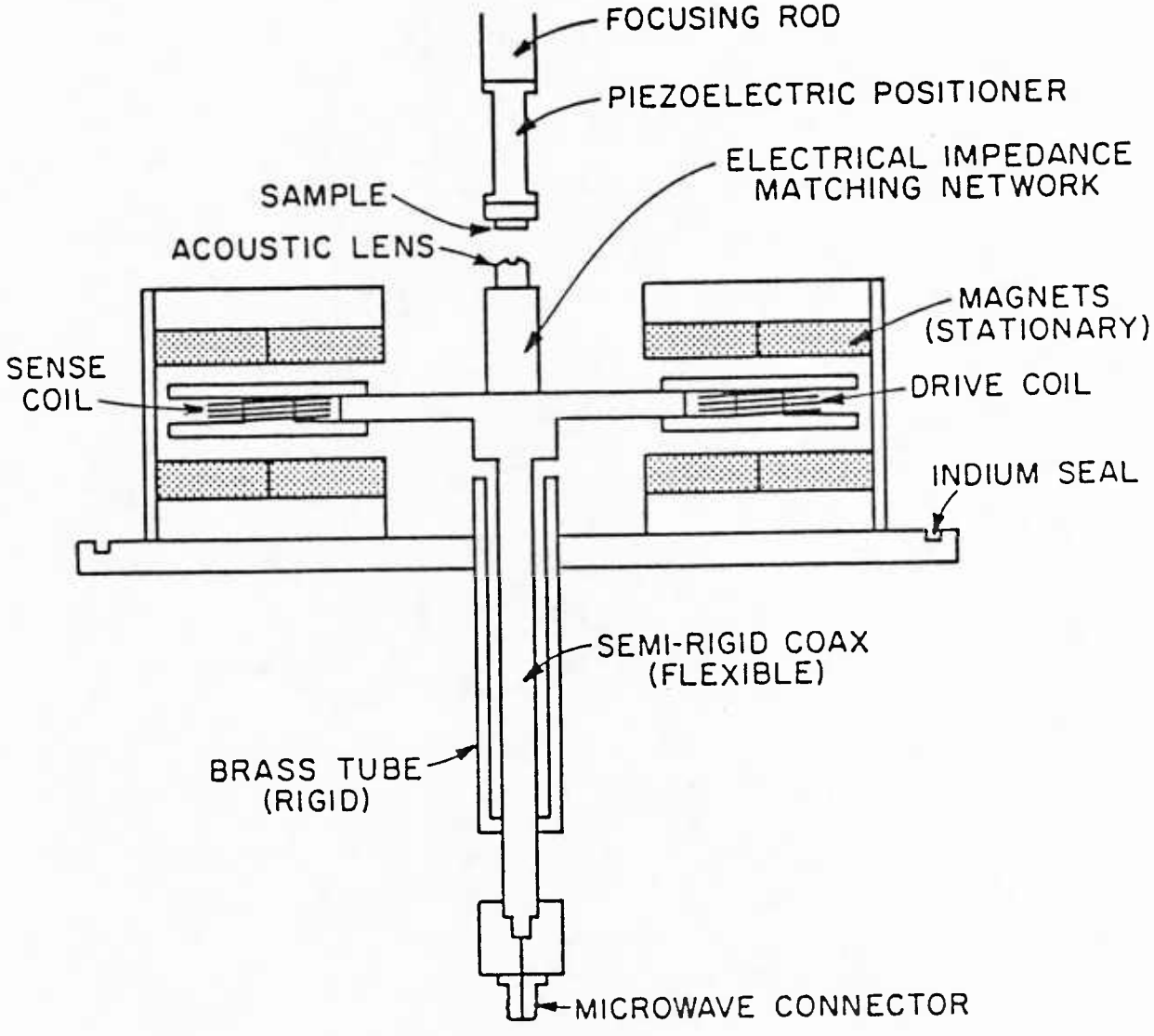

FIGURE 1.2-- Schematic diagram of the mechanical scanner used in conjunction with a dilution refrigerator.

Section 2, Nonlinearity) by transducer breakdown at typically 2 watts. An acoustic attenuation loss of 40 dB is acceptable in the water microscope. In most fluids the acoustic loss is given by[8]

$$\alpha = \frac{2\pi^2}{\rho c_o} \left(\frac{4}{3}\eta + \eta' + \kappa \left(\frac{1}{C_v} - \frac{1}{C_p} \right) \right) f^2 \qquad (1)$$

where ρ is the mass density, C_o is the sound speed, η is the shear viscosity coefficient, η' is the dilitational viscosity coefficient, κ is the thermal conductivity coefficient, and C_v and C_p are the specific heats at constant volume and pressure, respectively. Hence, increasing the frequency to obtain higher resolution quickly increases the acoustic attenuation. Because of this attenuation, the highest reported operating frequency of any acoustic microscope, except the very low temperature helium version, is 4.5 GHz.[2]

B. SUPERFLUID HELIUM

There exists a liquid, however, where the sound attenuation is negligible at microwave frequencies, that is, superfluid helium at temperatures less than 0.2 K. Figure 1.3 shows the acoustic attenuation in pure ^{4}He at 1 GHz. The dominant form of attenuation for low temperatures and $hf < kT$ is given by[9]

$$\alpha = 4.88 \cdot 10^{-3} \, fT^4 \text{ dB/cm}$$

where f is the frequency and T is the temperature in degrees Kelvin. Although acoustic attenuation will be covered in more detail in

Section 2, Fig. 1.3 clearly indicates that at sufficiently low temperatures, superfluid helium becomes essentially transparent to microwave frequency sound at 1 GHz.

The previous discussion justifies the use of superfluid helium for acoustic microscopy. However, before we continue with this subject, we will first take a brief moment to review some important characteristics of this "super" fluid. Helium-4 (the most common isotope) liquifies at its saturated vapor pressure at 4.2 K. Below 2.17 K (the λ-point) helium undergoes a second order phase transition and enters the superfluid phase. The superfluid phase can be described by two interpenetrating fluids, called the normal fluid and superfluid.[10] At 2.17 K, the fluid is all normal fluid, and the fraction of superfluid increases as the temperature decreases until the fluid is all superfluid at $T = 0$. The normal fraction acts as a "normal" thermo-viscous fluid, and can be associated with the excitations in the fluid. The superfluid fraction, however, can be associated with the quantum ground state. It has no viscosity and no entropy, so that it carries no heat. As the temperature is lowered below the λ-point, the number and energy of the excitations decrease. Below 0.5 K, the excitations are comprised of thermal phonons only, moving at the speed of sound with fairly long mean free paths. Thus, at these low temperatures, heat does not propagate diffusively but rather quasi-ballistically at the speed of sound. This accounts for the high thermal conductivity of low temperature helium.

The two-fold nature of superfluid helium gives rise to the possibility of fluid flow without resistance. As an example, superfluid

4165-1
(REV. A)

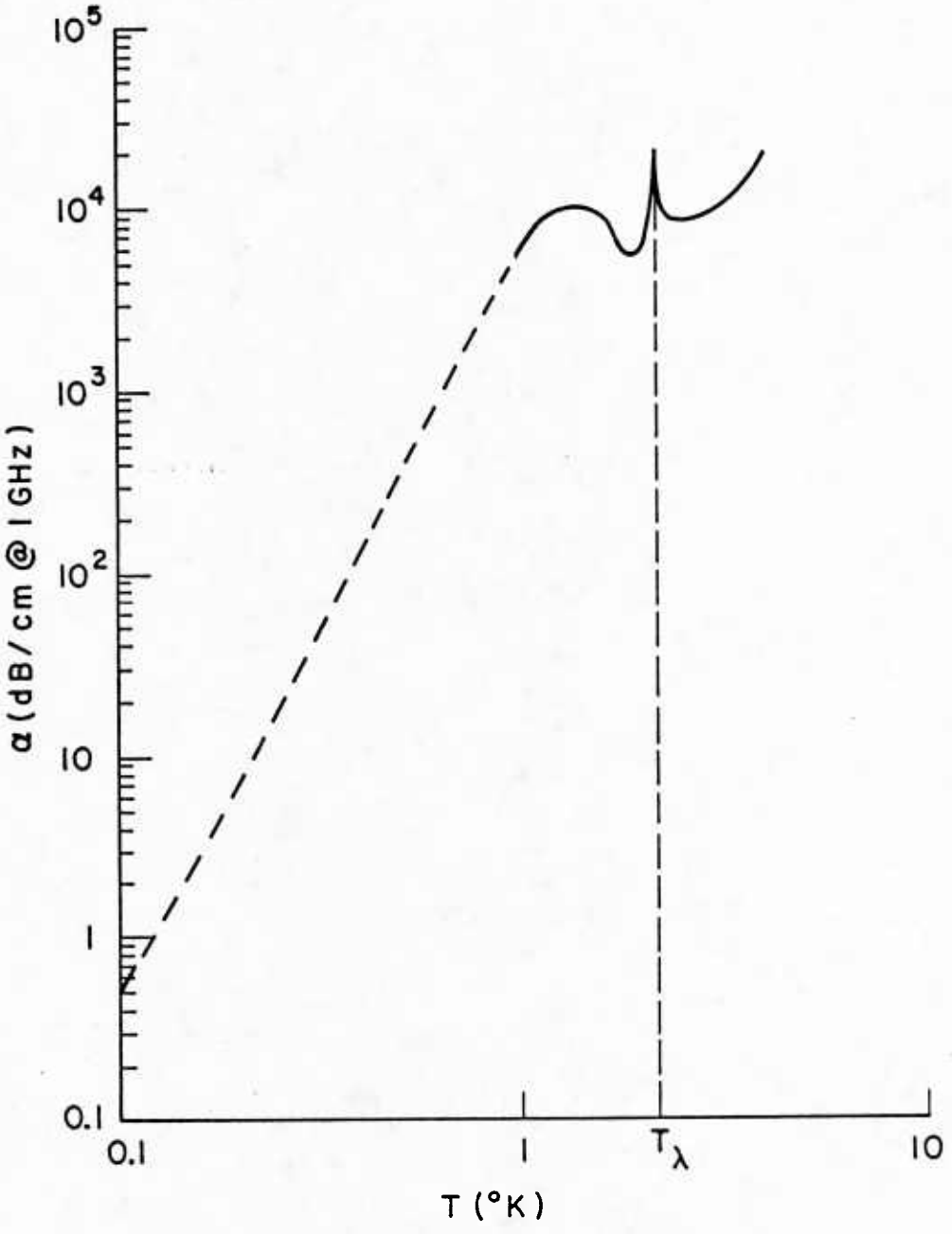

FIGURE 1.3--Sound attenuation in helium at 1 GHz.

films can move with no loss through extremely narrow passages, making leak-proof systems difficult to obtain. This film flow also complicates the refrigeration system used in this study, as we shall see in the next section.

C. REFRIGERATION

Helium-4 liquifies at 4.2 K at its saturated vapor pressure. The simplest method of cooling below this temperature is to pump on the liquid and cool by evaporation. However, at temperatures near 0.9 K, the vapor pressure of the helium is nearly zero, and the evaporation cooling power becomes negligible. An improvement can be made by using the isotope helium-3, but the lowest achievable temperature is $\approx$ 0.3 K. To achieve reasonable cooling powers at even lower temperatures, a dilution refrigerator is required.

The first operational dilution refrigerator was made in 1965.[11] Briefly, the refrigerator relies on the finite solubility (6.4%) of ^{3}He in ^{4}He at temperatures approaching zero. This finite solubility gives rise to a non-diminishing, effective vapor pressure of ^{3}He in a ^{3}He-^{4}He solution which allows cooling by pumping on the ^{3}He as in a normal evaporation refrigerator.[12]

The dilution refrigerator used in this study is the model 420-TL produced by S.H.E. Corporation, San Diego, CA. The refrigerator was installed and completely tested by J. Heiserman, then a research associate at Stanford University. The base temperature of the refrigerator is approximately 20 mK and the cooling power at 100 mK is greater than 0.15 mW. This refrigerator has one important feature for

use with the acoustic microscope--a top-loading design. The top loader consists of an access tube running down the cryostat into the experimental chamber where the lens and scanning assemblies are located. The sample is placed on a 7 foot long rod which slides through the access tube down into the experimental chamber (see Figure 1.2). With this arrangement, the sample rod may be removed from the refrigerator, the sample changed and the rod re-inserted, all while the dilution refrigerator is kept cold. A typical sample replacement takes just two hours. This compares favorably with the time required to cool the refrigerator (1.5 days) and warm to room temperature (2.5 days). We have used this sample changing feature to image as many as six samples in a single dilution refrigerator cooldown.

The top-loading option on the dilution refrigerator creates an experimental problem however. The acoustic microscope requires that the experimental chamber be filled with helium, and the helium tends to crawl up the top loading access tube toward room temperature. A superfluid film moving upward evaporates at the warmer parts of the tube and the gas molecules then condense at the colder parts, forming a large, undesirable heat leak to the experimental chamber. However, we can poison the superflow by using a dilute (2 to 3%) mix of ^{3}He in ^{4}He for the experimental solution. The ^{3}He adds viscosity to the superfluid and decreases the heat load on the experimental chamber.

Although the ^{3}He-^{4}He experimental solution has more acoustic attenuation than a pure ^{4}He solution, we shall see in Section 2 that the overall attenuation in the liquid path is small for the experiments performed thus far at low temperatures.

REFERENCES FOR SECTION 1

1. R.A. Lemons and C.F. Quate, in Physical Acoustics, W.P. Mason and R.N. Thurston, Eds. (Academic Press, New York, 1979), Vol. 14, pp. 1-92.
2. B. Hadimioglu and C.F. Quate, Appl. Phys. Lett. 43(11), 1006-1007 (1983).
3. J.S. Foster and D. Rugar, to be published in IEEE Trans. on Sonics and Ultrasonics.
4. B. Hadimioglu and J.S. Foster, submitted to J. Appl. Phys.
5. J. Heiserman, D. Rugar, and C.F. Quate, J. Acoust. Soc. Am. 67(5), 1629 (1980).
6. D. Ruger, J.S. Foster, and J. Heiserman, Acoustical Imaging, E.A. Ash and C.R. Hill, Eds. (Plenum Press, New York, 1982), pp. 13-25.
7. J.W. Goodman, Introduction to Fourier Optics (McGraw-Hill, New York, 1968), pp. 129,130.
8. K.A. Naugol'nykh, High Intensity Ultrasonic Fields, L.D. Rozenberg, Ed. (Plenum Press, New York, 1971), p. 5.
9. H.J. Maris, Phys. Rev. A 8, 2629 (1973).
10. S.J. Putterman, Superfluid Hydrodynamics (North-Holland Publishing Company, Amsterdam, 1974), pp. 1-32.
11. P. Das, R. De Bruyn Ouboter, and K.W. Taconis, Proc. 9th Intl. Conf. on Low Temp. Phys. (Plenum Press, London, 1965), p. 1253.
12. O.V. Lounasma, Experimental Principles and Methods Below 1K (Academic Press, London, 1974), pp. 17-58.

13. J.S. Imai and I. Rudnick, Phys. Rev. Lett. 22, 694 (1969).

14. B.M. Abraham, Y. Eckstein, J.B. Ketterson, M. Kuchnir, and J. Vignos, Phys. Rev. 181, 347 (1969).

2. TECHNICAL CONSIDERATIONS OF THE HELIUM ACOUSTIC MICROSCOPE

The superfluid helium acoustic microscope has been designed with many different technical considerations in mind. Acoustic attenuation, acoustic nonlinearity, and microwave noise comprise some of the critical areas which are covered in this section .

A. ATTENUATION

The acoustic attenuation in helium is dominated by two sources: scattering of sound by sound and scattering of sound by ^{3}He quasi-particles in the dilute ^{3}He-^{4}He experimental solution. We shall look at each of these in turn.

1. Scattering of Sound by Sound

Below 0.7 K, there are two sources of acoustic attenuation in pure ^{4}He, thermal phonon scattering and spontaneous decay of the acoustic phonons. Both of these are three-phonon processes. In the acoustic microscope experiments done thus far at Stanford, thermal phonon scattering dominates the attenuation. Figure 2.1(a) schematically shows the process in which an acoustic phonon and a thermal phonon collide and form a single higher energy phonon. The anomalous dispersion in helium at low pressure allows the conservation of energy and momentum for this process. Because the dispersion is small, however, the scattering angles are also small, typically less than a few degrees. The calculation of this scattering of sound by sound has been done by Westervelt[1] and generalized by Cabot and Putterman[2,3] allowing for

SOUND ATTENUATION IN HELIUM

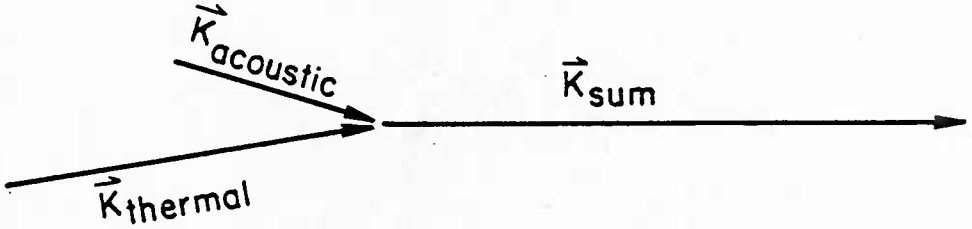

THERMAL PHONON SCATTERING

(a)

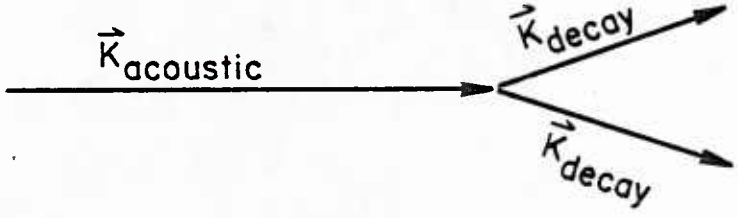

SPONTANEOUS DECAY OF PHONONS

(b)

FIGURE 2.1--The scattering processes which lead to sound attenuation in superfluid helium below 0.5K.

dispersion. The result for the power attenuation is[2]

$$\alpha_{th} = \frac{\pi^2}{\rho c^2}(1 + \mu_o)^2 \, I\left[\int_0^\infty \frac{(k_a + k)^2}{k} E(K)dk - \int_{k_a}^\infty \frac{(k_a - k)^2}{k} E(K)dK + \int_0^{k_a} \frac{(k_a - k)^2}{k} E(K)dk\right]$$

where ρ is the helium density, c is the sound speed, μ_o is $\frac{\rho}{c}\frac{dc}{d\rho}$ ($\simeq 3.84$ at low pressure), k_a is the acoustic wavenumber $= w/c$, k is the thermal wavenumber, $E(k)$ is the energy density in the liquid per unit wavenumber and per solid angle in the $\vec{k}_a$ direction, and the value of I depends on the dispersion. For the dispersion in helium at its saturated vapor pressure, (see Reference 2) $I \simeq 2$.

The attenuation α_{th} includes three terms, each of which corresponds to a specific process. The first term is the process shown in Fig. 3(a) and represents the generation of a phonon with wavenumber $k + k_a$. The second term corresponds to generation of a phonon with wavenumber $k - k_a$ (difference frequency) and it is negative, indicating that amplification occurs for this process if $k > k_a$. The third term again corresponds to difference frequency generation, which is a loss when $k < k_a$.

In the case where $hw \ll kT$, the third term in α_{th} become small, and the lower limit on the second integral can be approximated by 0. Then the first two terms can be combined easily and the result is

$$\alpha_{th} = \frac{\pi(1 + \mu_o)^2 I}{\rho c^3} w E_{ph}$$

where E_{ph} is the energy density of the thermal phonons in the superfluid = $4\pi \int_o^\infty E(k)dk$. The above expression for the attenuation is a good approximation for α_{th} unless $hw \gtrsim 5$ kT , and all three terms in α_{th} must be calculated.

The energy density of the thermal phonons can be related to the temperature in a simple way. The energy density is

$$E_{ph} = \int np \frac{\partial \varepsilon}{\partial p} d\tau_p$$

where n is the distribution function of the gas of thermal phonons = $[\exp(\varepsilon/kT) - 1]^{-1}$, ε is the energy of a thermal phonon, k is Boltzmann's constant, p is the phonon momentum and $d\tau_p = p^2 dp d\Omega / h^3$. If we let $\varepsilon = cp$ (assuming linear dispersion), we find the energy density is

$$E_{ph} = \frac{4\pi^5 (kT)^4}{15\, h^3 c^3}$$

The attenuation can then be written ($I \approx 2$) :

$$\alpha_{th} = \frac{8\pi^6 (1 + \mu_o)^2}{15\, \rho\, c^6\, h^3} w (kT)^4 \quad .$$

The T^4 behavior comes about because that is the temperature dependence of the energy density of the thermal phonons in the helium. The above

expression is a good approximation for α_{th} unless $\hbar\omega \gtrsim 5$ kT (10 GHz at 0.1K), and all three terms in α_{th} must be calculated.

The data in Fig. 2.2 demonstrates the temperature dependence of the attenuation of high frequency sound in superfluid helium due to thermal phonon scattering. The line drawn through the data corresponds to T^4 dependence. The acoustic frequency was 4.2 GHz and represents the highest frequency used in helium attenuation experiments.

The other three-phonon scattering process in superfluid helium is the spontaneous decay of acoustic phonons. This process may be interpreted as the scattering of ultrasonic phonons by zero point motion of the helium. This causes the acoustic phonon to split into two lower frequency phonons as shown schematically in Fig. 2.1(b). At saturated vapor pressure and low acoustic intensities, the attenuationor is[4]

$$\alpha_{sd} = 3.3 \cdot 10^{-50} f^5 \text{ dB/cm} \quad .$$

In practice, spontaneous decay attenuation only becomes important for acoustic microscopy above 20 GHz.

2. Scattering of Sound by ^{3}He Quasiparticles

Because of the refrigeration requirements of the superfluid helium acoustic microscope, a dilute solution of $\approx 3\%$ ^{3}He-^{4}He must be used instead of pure helium-4 in the experimental chamber. Beyond the attenuation mechanisms discussed in the last section, there is an additional attenuation due to the ^{3}He quasiparticles. The two types of scattering which contribute to the attenuation are phonon absorption by

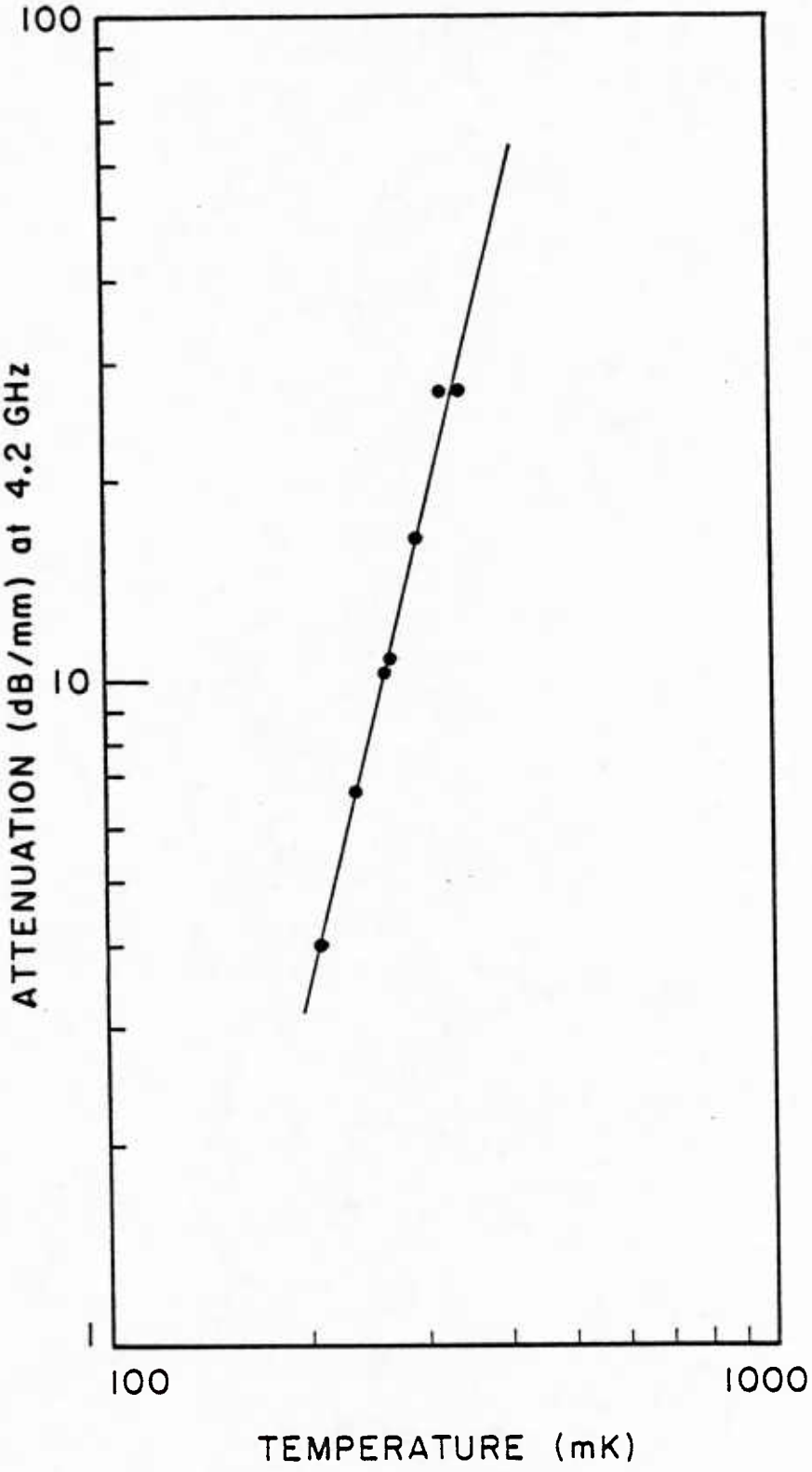

FIGURE 2.2--Sound attenuation at 4.2 GHz.

the ^3He quasiparticles mediated by quasiparticle-quasiparticle interactions, and Rayleigh-like scattering of the phonons by the ^3He quasiparticles.

For the phonon absorption process to occur, a quasiparticle-quasiparticle interaction is essential, because energy-momentum conservation forbids phonon absorption by a subsonic particle. (For the ^3He particle densities considered here, $V_f << c$ where V_f is the ^3He Fermi velocity, c is the sound speed.) Quasiparticle interactions allow the sharing of the phonon energy and momentum among several quasiparticles.[5,6] The phonon absorption attenuation is independent of frequency in the gigahertz range and for a 5% ^3He-^4He solution is calculated to be[5]

$$\alpha_{abs} = 5.6 \times 10^3 T^2 \text{ dB/cm}$$

The Rayleigh-like scattering of phonons is a quasi-elastic process. Thus the only effect of the scattering is only to change the direction of the incident phonon. For a coherent transmitting and receiving system, however, even a very small change in the phonon direction will act as an attenuation of the signal. The effective attenuation then becomes (for 5% ^3He-^4He)[5]

$$\alpha_{qp} = 8.2 \times 10^{-3} f^4 \text{ dB/cm}$$

where f is the sound frequency in gigahertz.

Although the attenuation of ultrasound in ^{3}He-^{4}He mixtures is usually considered to be due to the quasiparticle phonon absorption, we see that at low temperatures and high frequencies, Rayleigh-like scattering also contributes. At a frequency of 8 GHz,[7] (the present operating frequency of the acoustic microscope), the two forms of attenuation are equal at 77 mK. To the author's knowledge, no direct measurement of the attenuation due to the Rayleigh-like scattering has ever been made.

It is clear from the attenuation discussion that very low temperatures are required to minimize the attenuation of sound in the acoustic microscope. At a typical operating temperature of 100 mK in the dilution refrigerator, the total attenuation in helium due to the processes described above is less than 4 dB over the path required by the 8 GHz acoustic microscope (0.4 mm).

B. NONLINEARITY

Whereas the attenuation of sound in superfluid helium can be virtually eliminated using modern refrigeration techniques, the nonlinearity of sound propagation is a more fundamental problem, since it limits the effective acoustic input intensity. Depletion of the transmitted acoustic beam occurs due to wave profile distortion (harmonic generation), leading to saturation of the received power for sufficiently high transmitted power.[8,9] This saturation effect gives rise to an effective maximum input power (typically < 1 nW) which is far less (in helium) than the input power limited by transducer burnout. Thus, the potential signal-to-noise ratio of the microscope is reduced significantly by the nonlinear effect.

Figure 2.3 shows the variation of the profile of a finite amplitude plane wave during propagation in the lossless case.[10] The propagation of an originally sinusoidal wave distorts with time and distance. There are two sources of the distortion: convection and nonlinearity in the equation of state connecting the pressure and the density. For small distances from the sinusoidal source, the distortions of the wave are small. However, at a distance

$$L = \left[\frac{\rho c^5}{8\pi^2(1+\mu_o)^2 I_n f}\right]$$

(where L is the discontinuity length, and I_n is the acoustic intensity) the solution to the wave profile in the vicinity of $\rho = 0$ becomes vertical [Fig. 2.3(b)], and then multivalued [Fig. 2.3(c)]. But this situation is physically impossible since it implies several densities at the same position. In fact, Fig. 2.3(b) indicates the formation of a discontinuity (weak shock wave). Depletion of the shock wave arises from the irreversible loss of the "spillover" of the wave[11] [Fig. 2.3(c)] which can also be calculated as an attenuation of the higher Fourier components of the sound wave.[12] Figure 2.3(d) shows the characteristic sawtooth wave which forms at long distance. The onset of a discontinuity produces strong attenuation of the wave. Physically this damping (for normal fluids) is attributable to irreversible compression processes in the shock wave and the attendant increases in the entropy and dissipation of energy.[10] For distances much greater than L, the amplitude of the sawtooth no longer depends on the initial amplitude since the absorption increases with the wave intensity. We

VARIATION OF THE PROFILE OF A FINITE-AMPLITUDE SOUND WAVE DURING PROPAGATION

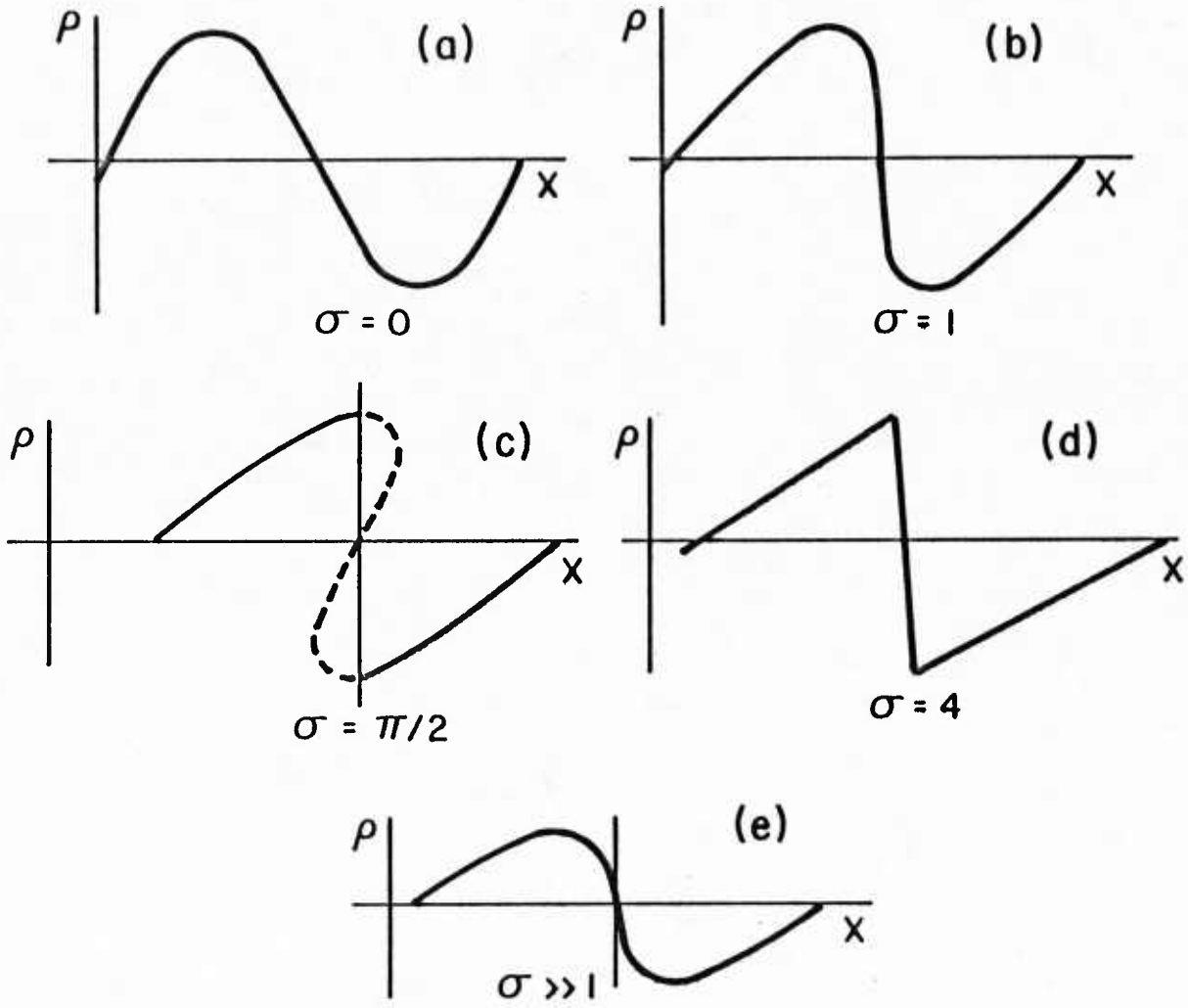

FIGURE 2.3

can estimate the saturation power by considering the power lost to the second harmonic. For a tightly focused beam when the nonlinear harmonic generation is not too strong, the power in the second harmonic is given by[13]

$$P_2 = \frac{16\pi^3(1 + \mu_o)^2}{\rho_o c^5} F^2 f^2 [P_1(0)]^2$$

where ρ_o is the density of the liquid, c is the sound speed, μ_o is $\frac{\rho}{c}\frac{dc}{d\rho}$, F is the f-number of the lens, f is the transmitted frequency, and $P_1(0)$ is the fundamental input power.

Defining the "onset" of significant nonlinearity to be when $(P_2/P_1(0)) = 0.1$, we have

$$P_{onset} = \frac{0.1}{F^2 f^2} L_f$$

where L_f is a constant characterizing the linearity of the liquid for focused beam propagation and is given by

$$L_f = \frac{\rho_o c^5}{16\pi^3(1 + \mu_o)^2}$$

P_{onset} is a crude estimation of the saturating power for the focused system of the acoustic microscope. The parameter L_f gives us an indication of why nonlinearity in helium is a large problem. Helium has a very low density (1/7 of water) and a low sound speed (again 1/7 of water). These two factors change L_f by about 50 dB from water to helium. The two factors giving rise to the nonlinearity, convection and

a nonlinear equation of state, are represented by the term $(1 + \mu_0)$, and we see they are additive. For helium at its saturated vapor pressure, $\mu_0 \approx 3.84$, not appreciably different from other fluids. For a lens with an F-number equal to 1, operating at 4.2 GHz, the theoretical transmitted power for the onset of depletion in helium is only $8.6 \cdot 10^{-11}$ W. Since the received power at full saturation is only several fold greater than this, it is obvious that care must be taken in order to achieve an acceptable signal-to-noise ratio. It should be noted that P_{onset} falls 6 dB per doubling of the operating frequency, implying that acceptable signal-to-noise ratio of the microscope becomes increasingly more difficult to achieve at higher frequencies.

Figure 2.4 shows the results of a high intensity plane-wave transmission experiment done in pure helium-4 at a temperature of 50 mK. The output intensity is plotted as a function of input intensity for several propagation distances. The frequency is 3.25 GHz. We see that the simple saturation effect expected for normal fluids and seen experimentally for higher temperature helium[14] does not occur. In fact, as saturation begins to occur, the output intensity actually begins to roll off, and we obtain less power out as more power is put in. A simple explanation for the results in Fig. 2.4 goes as follows: In normal fluids the acoustic loss goes into a local entropy increase (heat) which remains behind the propagating wave. In other words, a shock wave leaves the fluid behind warmer than the fluid in front of the wave. In superfluid helium at low temperatures, however, any increase in entropy is associated with long mean free path "thermal" phonons, which propagate at the sound speed and therefore move with the shock

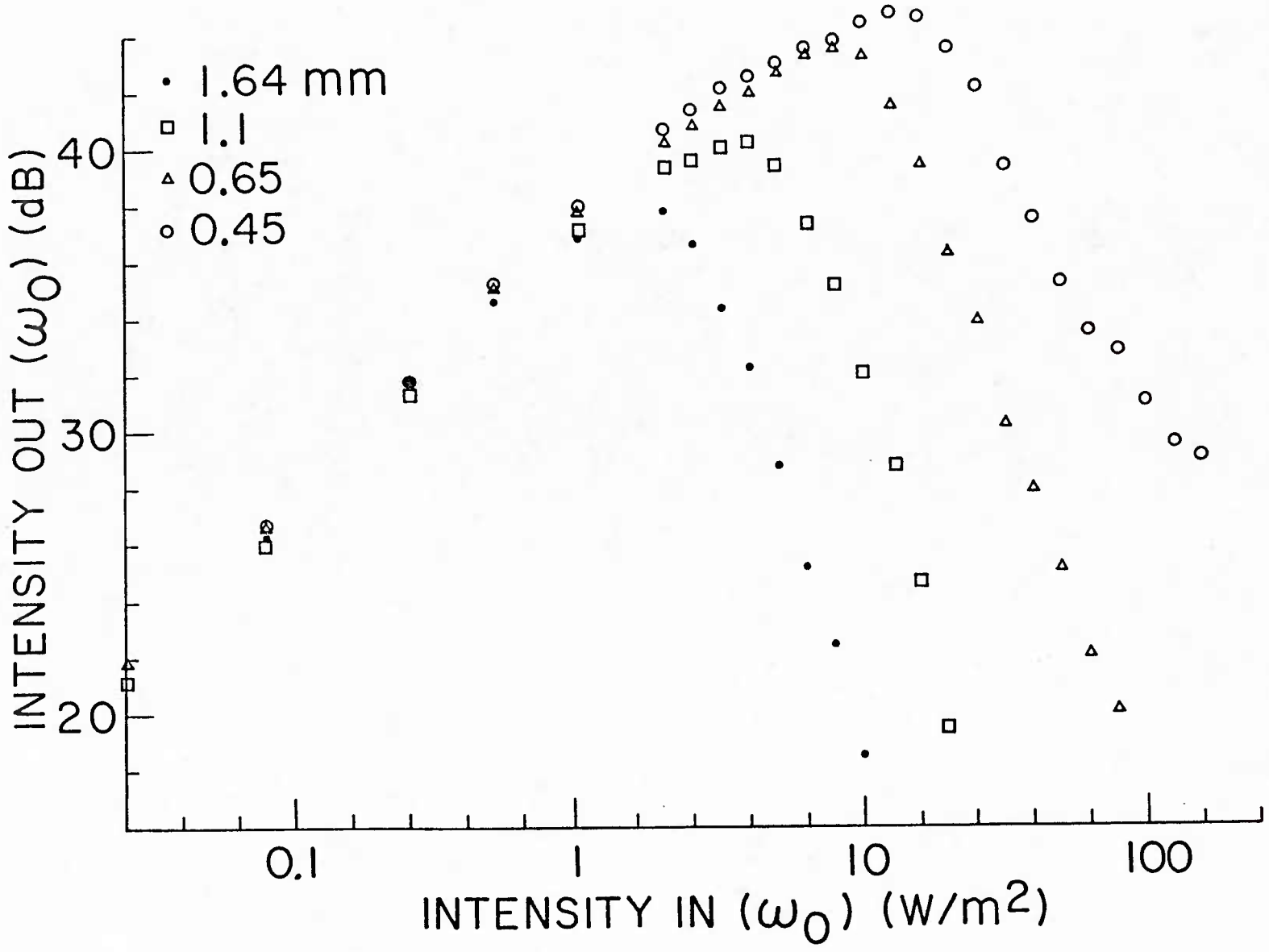

FIGURE 2.4--High intensity plane wave transmission in low temperature helium.

wave. If we consider momentum conservation, the depleting shock wave must actually emit all phonons in the same direction as the moving shock, ignoring dispersion effects and any breakdown in superfluidity. These emitted phonons can act to scatter the transmitted phonons via the three-phonon processes described in Section A of this chapter, and deplete the transmitted beam of acoustic phonons. Figure 2.4 points out an essential difference between intense sound propagation in normal liquids and low temperature superfluid helium. This topic is now under active consideration and is the subject of ongoing research at Stanford.[15]

C. SIGNAL-TO-NOISE IMPROVEMENTS IN THE ACOUSTIC MICROSCOPE

In Section B, we saw that there was a severe limitation in the effective acoustic input power in the helium acoustic microscopy. To optimize the signal-to-noise ratio of the microscope, we must maximize the efficiency of the acoustic receiving system and minimize the noise of the system. Because of the nonlinearity in the helium, the acoustic transducer need not be optimized for illumination of the lens as has been previously described.[16] The saturation effect allows every region of the lens to produce the same maximum acoustic intensity. Thus, the transducer must be optimized to efficiently receive the reflected signal from the sample. Typical lens parameters to accomplish this task are given in section 4, and improvements of several decibels are seen over conventionally designed lens assemblies.

Noise improvements, however, have been far more important than lens improvements in the successful construction of the superfluid helium acoustic microscope. The noise in the system is the sum of the thermal

source noise (from the microscope and any lossy line connecting the microscope to the pre-amplifiers) and the noise of the pre-amplifiers. The thermal noise of the microscope is negligible because the temperature is so low, typically $T < 0.1$ K. The coaxial line connecting the microscope to the pre-amplifiers is superconducting and virtually lossless at microwave frequencies. Thus, the RF pre-amplifiers set the noise temperature of the receiving system. To minimize this noise, GaAs FET amplifiers have been designed to operate in the 4.2 K helium bath of the dilution refrigerator.[8,17] These cooled pre-amplifiers were designed and constructed for experiments at 2.6, 3.2, 4.2, and 8.0 GHz.[18] A schematic of a pre-amplifier is shown in Fig. 2.5. The noise temperature of the helium-cooled amplifiers (and the receive system) at 4.2 GHz is approximately 20 K. This provides an increase of 20 dB in the noise performance over room temperature microwave amplifers.

To match the low impedances of the gate and drain of the FET to 50 ohms, microstrip lines are used at the input and output of the amplifier, as shown in Fig. 2.5. Quarter-wave microstrip sections match the real impedances while the capacitance of the gate and drain are cancelled at the appropriate frequency by varying the inductance of their respective leads. Capacitors are used at the amplifier input and output to block the d.c. voltages on the transistor. Bias circuits are connected to the gate and drain by wire coils with a large RF impedance. Typical gain from a single amplifier is 10-15 dB, and several stages are usually used to obtain enough gain to realize the potential increase in noise performance over room temperature operation.

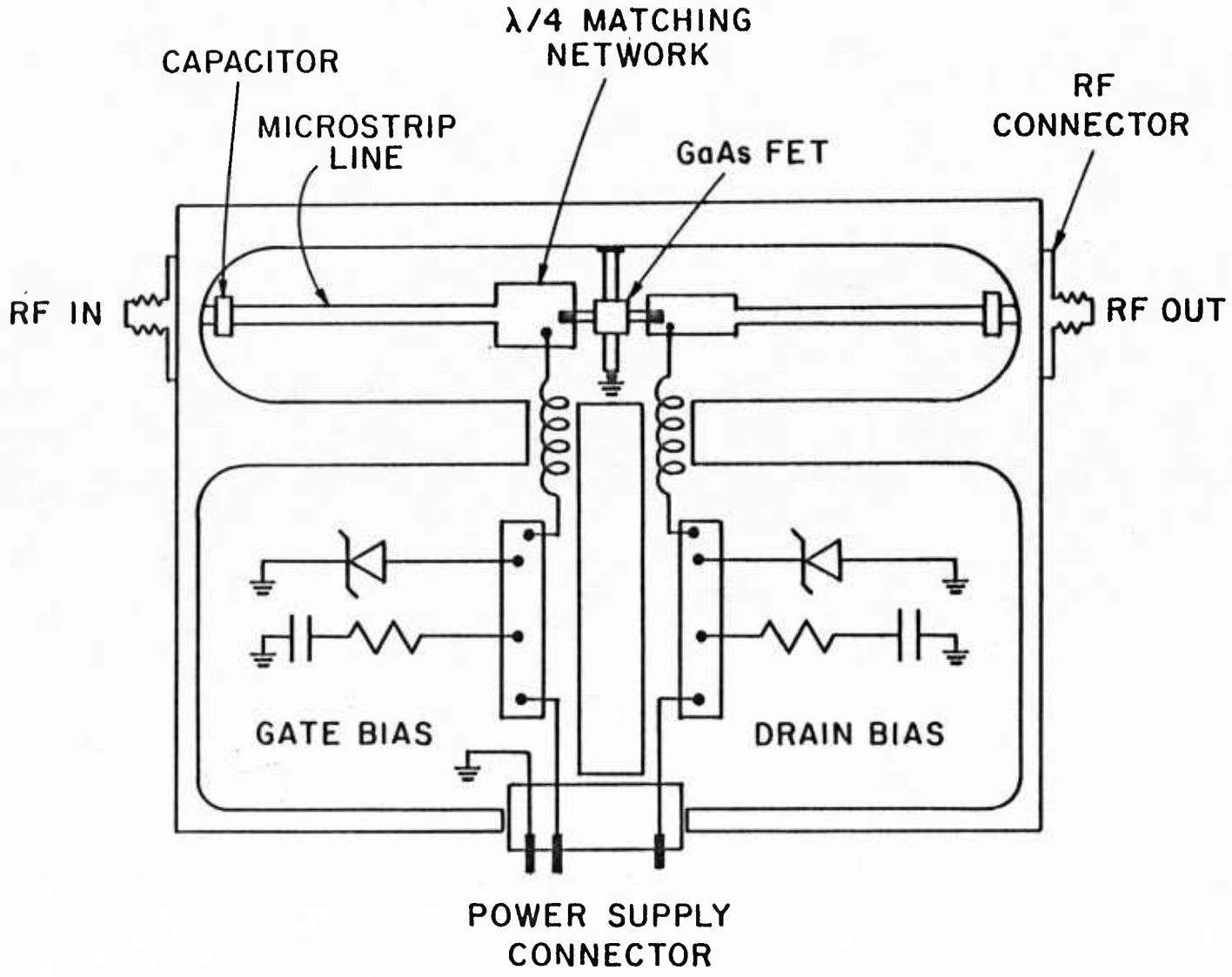

FIGURE 2.5--Helium-cooled low-noise microwave amplifier.

5178-23

Pulse expansion and compression techniques have also been used to improve the signal-to-noise ratio of the helium acoustic microscope.[7] Since the nonlinearity of the liquid sets a limit on the input power, it is quite natural to turn to pulse compression techniques which are widely used in radar systems where the peak power is limited by the transmitting power amplifier. The system allows one to use a pulse of small amplitude and long duration in the transmitting system and convert it to a high amplitude short duration pulse in the receiving system. The dispersive filters used for expansion and compression are surface acoustic wave devices with a time-bandwidth product of approximately 200, and the measured improvement in the signal-to-noise ratio with the filters is 18 dB. A block diagram of the electronic system used at 8.0 GHz is shown in Fig. 2.6 (courtesy of B. Hadimioglu).[7]

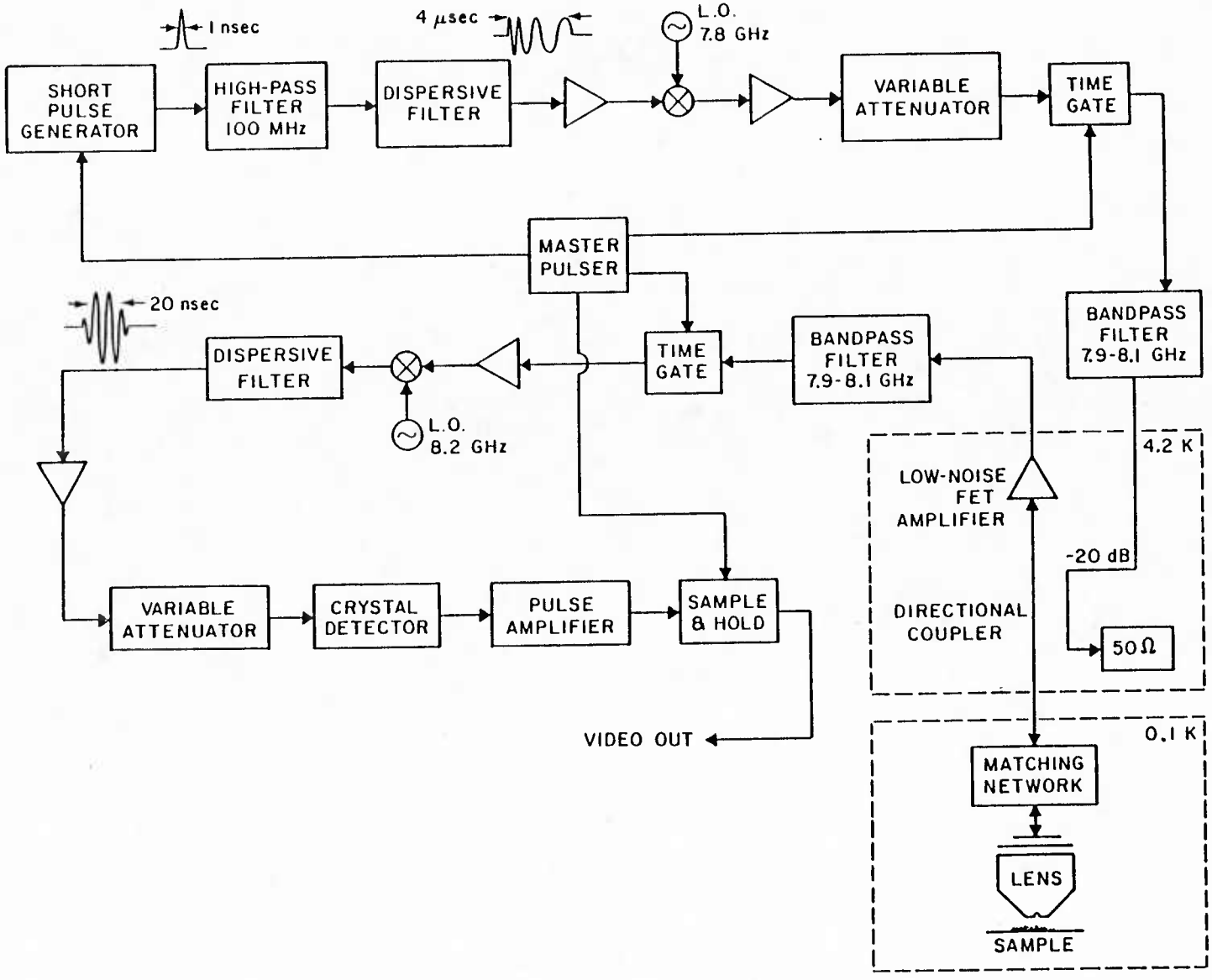

FIGURE 2.6--Electronic system for the acoustic microscope at 8 GHz.

5179-1

REFERENCES FOR SECTION 2

1. P.J. Westervelt, J. Acoust. Soc. Am. 59, 760 (1976).
2. M. Cabot, Ph.D. Dissertation, UCLA (1983).
3. M. Cabot and S. Putterman, Phys. Lett. 83A, 91 (1981).
4. M. Cabot and S. Putterman, Physica B & C 107, No. 1, Proceedings of the 16th International Conference on Low Temperature Physics, 107-108 (1981).
5. G. Baym and C. Ebner, Phys. Rev. 164, 235 (1967).
6. T. McMullen, J. Low Temp. Phys. 51, No. 1/2, 33 (1983).
7. B. Hadimioglu and J.S. Foster, submitted to J. Appl. Phys.
8. J.S. Foster and D. Rugar, Appl. Phys. Lett. 42(10), 869 (1983).
9. D. Rugar, J. Appl. Phys. (in press).
10. K.A. Naugol'nykh, High Intensity Ultrasonic Fields, L.D. Rozenberg, Ed. (Plenum Press, New York, 1971), pp. 15-22.
11. L.D. Landau and E.M. Lifshitz, Fluid Mechanics (Pergamon Press, London, 1959), pp. 372-377.
12. D.T. Blackstock, J. Acoust. Soc. Am. 39, No. 6, 1019 (1966).
13. J.S. Foster and D. Rugar, to be published in IEEE Trans. on Sonics and Ultrasonics.
14. A. Hikata, H. Kwun, and C. Elbaum, Phys. Rev. B 21, No. 9, 3932 (1980).
15. J.S. Foster and S. Putterman, to be published.
16. V. Jipson, Ph.D. Dissertation, Stanford University (1979).
17. S. Weinreb, IEEE Trans. Microwave Theory Tech. 28, 1041 (1980).
18. B. Hadimioglu constructed the 8 GHz preamplifiers.

3. ACOUSTIC MICROSCOPY IN LIQUID NITROGEN AND LIQUID ARGON

A. INTRODUCTION

Although liquid helium is the liquid of choice for extending the resolution of the acoustic microscope to its ultimate limits, other cryogenic liquids offer great promise for use in acoustic microscopy. Two liquids in particular, liquid nitrogen and liquid argon, have been used very successfully. These two liquids have figures of merit of 2.2. Liquid nitrogen is readily obtainable in most laboratories and is inexpensive. Liquid argon is commercially available, although it is somewhat more costly than nitrogen. These liquids require minimal cryogenic apparatus since they can be used at atmospheric pressure. Furthermore, they have acoustic impedances which are relatively high. This quality greatly simplifies the impedance matching problem which is so troublesome in the design of acoustic lenses for helium.

This chapter discusses the design and performance of the acoustic microscope operating in nitrogen or argon. In Section B the acoustic properties of liquid nitrogen and liquid argon are reviewed. Section C describes the design of a lens with 18 μm radius which can be used at frequencies as high as 2.8 GHz. Section D presents and interprets images of a variety of objects that were viewed in liquid nitrogen or argon. In most cases, resolution comparable to that obtainable using optical microscopy is observed. The objects examined in the nitrogen/argon microscope include test patterns, GaAs field effect

transistors, human metaphase chromosomes and chick heart fibroblasts.

B. PROPERTIES OF LIQUID NITROGEN AND LIQUID ARGON

Some physical properties of liquid nitrogen and liquid argon are given in Table 3-1.

TABLE 3-1

Some Properties of Argon and Nitrogen[1,2]

	Argon	Nitrogen
Normal boiling point:	87.29K	77.35K
Triple point temperature:	83.78K	63.15K
Triple point pressure:	516 Torr	94 Torr
Density:	1.37 g/cm^3	0.81 g/cm^3

Nitrogen exists in its liquid state at atmospheric pressure in the temperature range between about 63K and 77K. For use in acoustic microscopy, the liquid was primarily used near the normal boiling point. To reduce the bubbling of the liquid due to boiling, a double Dewar cryostat was used with both inner and outer vessels filled with liquid nitrogen. In this configuration, the heat leak into the inner

vessel is very small and the small amount of boiling which occurs does not interfere with picture taking. It is also possible to slightly overpressure the nitrogen in the inner Dewar so that it is kept below its boiling point by the nitrogen in the outer jacket. Liquid argon exists only in the narrow temperature range 84 - 87K at atmospheric pressure. Boiling of the liquid is prevented altogether by the presence of liquid nitrogen in the outer jacket of the Dewar. In fact, care must be taken to prevent the argon from freezing.

Liquid nitrogen and argon have the advantage over liquid helium in that they have relatively higher acoustic impedances. The acoustic impedance of liquid argon is 1.2×10^5 g/cm^2-s. This is 40 times larger than the impedance of helium and is close to the value for water, 1.5×10^5 g/cm^2-s. The impedance of liquid nitrogen is somewhat smaller, 0.68×10^5 g/cm^2-s.

The acoustic attenuation, α/f^2 , in liquid nitrogen is 13.8×10^{-17}s^2/cm or 12.0×10^{-16} dB-s^2/cm. The attenuation in liquid argon is 15.2×10^{-17}s^2/cm or 13.2×10^{-16}dB-s^2/cm. These values are somewhat higher than the value for hot (60°C) water, $\alpha/f^2 = 10.9 \times 10^{-17}$s^2/cm. This means that, in general, the liquid nitrogen/argon microscope must operate at somewhat lower frequencies than a microscope using hot water. It is interesting to note that the attenuation in nitrogen/argon is about equal to that of water at biological temperatures, 35-40°C. Thus acoustic lenses that are optimized in terms of frequency of operation for use in nitrogen or argon will perform excellently as lenses for studying living biological objects in water and vice-versa.

C. LENS DESIGN

This section discusses the design of acoustic lenses for use in nitrogen or argon. Special attention is given to impedance matching and lens illumination. Many principles of water lens design are applicable to the design of nitrogen/argon lenses. For background information on the general considerations, works by Lemons,[3] Jipson,[4] Atalar,[5] and Bray[6] may be consulted.

C.1. Impedance Matching

Because of the more moderate impedance values of nitrogen and argon, many of the impedance matching difficulties encountered in the helium case are avoided. The first lenses used in our experiments utilized quarter-wavelength glass layers, identical to the glass layers used for microscopy in water. These layers are discussed by Jipson.[4] The impedance of sputtered 9741 borosilicate glass (Corning Glass Works) is approximately $11.6 \times 10^5 g/cm^2\text{-}s$. The output impedance of the sapphire-glass combination can be determined with a straightforward calculation. This gives $Z_0 = 3.0 \times 10^5 g/cm^2\text{-}s$. The power transmission coefficient for traversing a sapphire-nitrogen interface with a glass matching layer is,

$$T_{N_2} = 0.60 = -2.2 \text{ dB}$$

and the corresponding value for the argon case is

$$T_{Argon} = 0.82 = -0.9 \text{ dB}$$

A better impedance match can be obtained if the evaporated amorphous carbon layer is used as a matching layer. If a layer impedance of $8 \times 10^5 g/cm^2\text{-}s$ is assumed, the output impedance is $Z_0 = 1.44 \times 10^5 g/cm^2\text{-}s$. The power transmission coefficients into nitrogen and argon are then given by

$$T_{N_2} = 0.87 = -0.6 \text{ dB}$$

$$T_{Argon} = 0.99 = -0.04 \text{ dB}$$

A plot of power transmission as a function of frequency is shown in Fig. 3-1. The 3-dB transmission bandwidth of the matching layer is seen to be about 35%. Because of the broad bandwidth, the cosine thickness profile on the surface of a lens does not significantly degrade matching layer performance.

C.2. Lens Illumination

We consider here a sapphire lens with 18 μm radius and an opening half-angle of 53°. The aperture radius of such a lens is about 14 μm. If the sapphire rod is 1.25 mm long and a 116 μm diameter transducer is excited at 2.6 GHz, the acoustic field pattern at the plane of the lens will be like that shown in Fig. 3-2. The -3 dB point of the pattern occurs at $r = 17$ μm . At the edge of the lens aperture the amplitude is 2.1 dB below the on-axis value. Approximately 25% of the power radiated by the transducer falls within the lens aperture. This results in a two-way illumination loss of -12 dB. The phase of the illumination is constant to within 0.02 radian accross the aperture.

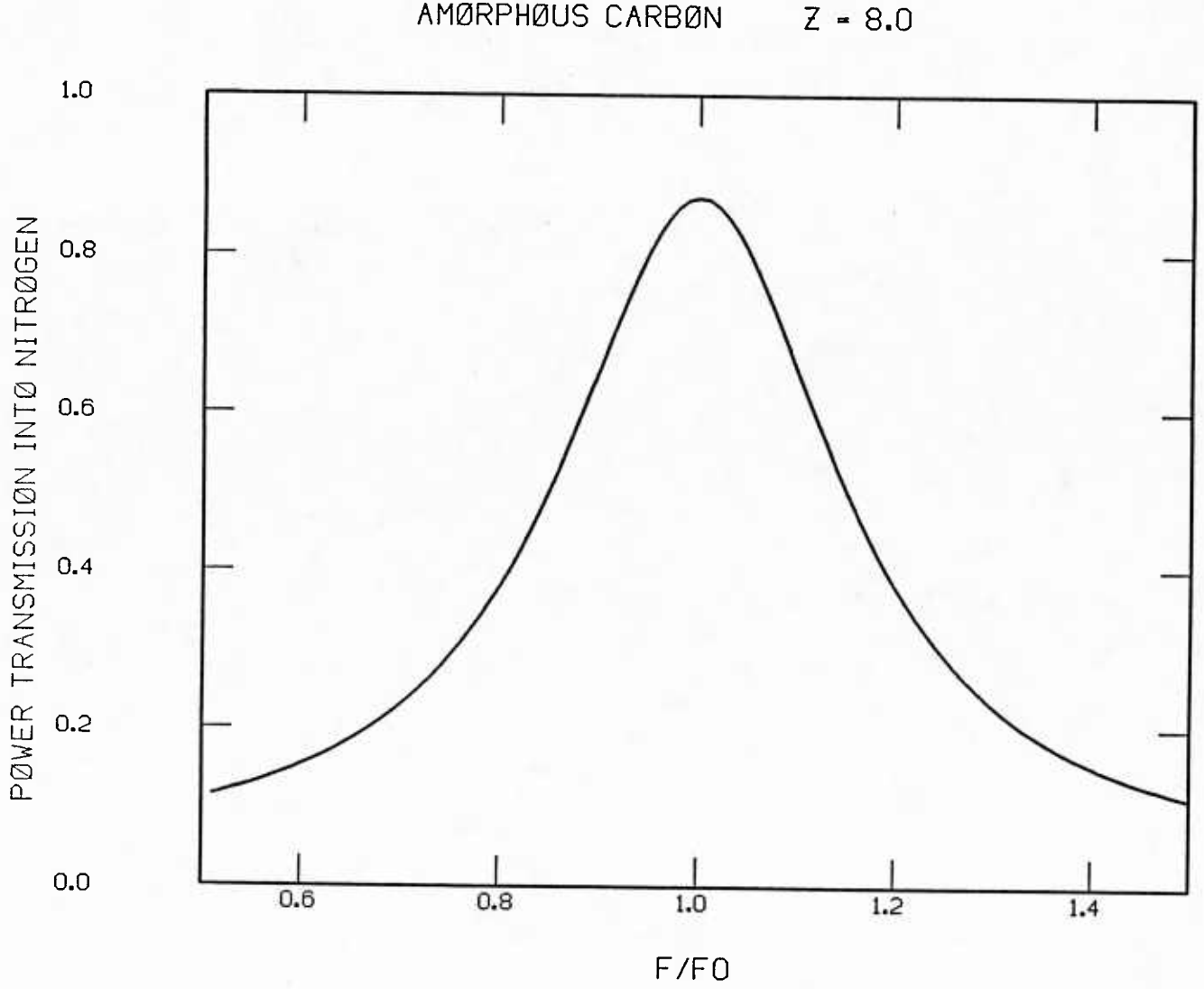

FIGURE 3.1--Transmission into liquid nitrogen as a function of frequency for amorphous carbon matching layer ($Z = 8.0 \times 10^5$ g/cm^2 -s) on sapphire.

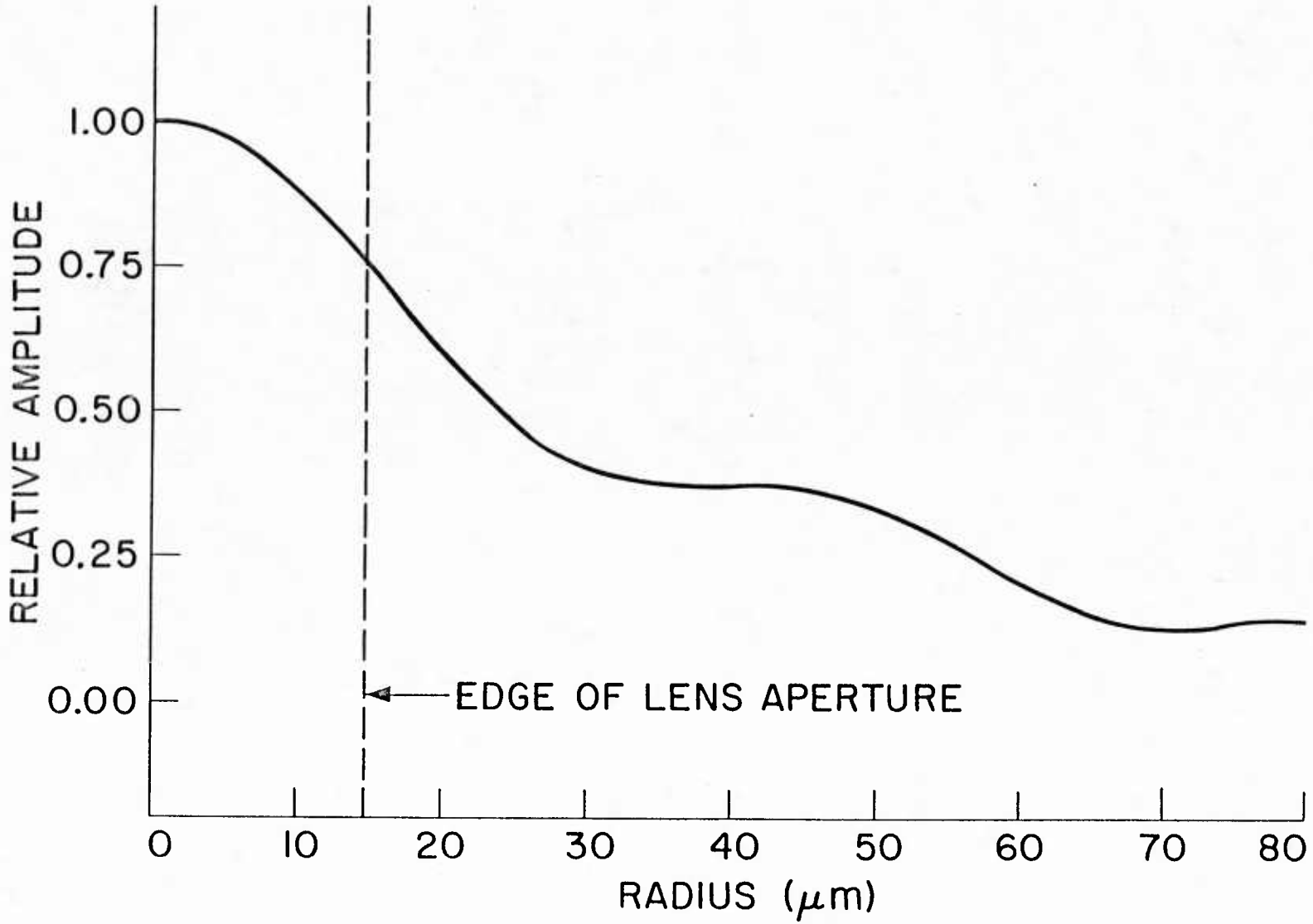

FIGURE 3.2--Acoustic field distribution at lens plane for nitrogen lens. Sapphire rod is assumed to be 1.25 mm long. The transducer is assumed to have a diameter of 116 μm and to be operating at 2.6 GHz.

C.3. Design of a 2.6 GHz Lens

This section describes the design of an acoustic lens optimized for operation at 2.6 GHz. Good images may be taken with the lens in the frequency range from 2.0 to 2.8 GHz. At the center frequency, 2.6 GHz, the signal-to-noise ratio is better than 30 dB for a 10 mW RF input. The characteristics of the lens are given below.

Summary of Lens Characteristics:

- Operating Frequency: 2.0 - 2.8 GHz
- Wavelength in Nitrogen: 4200-3000 Å
- Physical:
  - Material: Sapphire
  - Lens radius: 18 μm
  - Lens opening half-angle: 53°
  - Rod length: 1.25 mm
  - Rod diameter: 0.25 inch
- Matching Layer:
  - Material: Amorphous carbon deposited at 350°C
  - Interface layers: 200 Å Ti, 1000 Å Mo
  - Center frequency: 2.5 GHz
  - Layer impedance: 7.4×10^5 g/cm^2-sec
  - Output impedance: 1.25×10^5 g/cm^2-sec
  - Two-way interface loss in N_2 (plane waves): -0.8 dB

Transducer:

Material: Sputtered ZnO

Counter electrode: Gold

Top electrode: 116 μm diameter top dot w/offset bond pad

Two-way conversion loss: -11 dB

Lens illumination loss (2-way): -12 dB

[a] Pulse Timing:

RF to LL: 230 nsec

LL to signal: 40 nsec

LL to LS: 105 nsec

LL to LLLL: 230 nsec

Pulse Heights at 2.6 GHz in LN_2 :

Insertion loss (signal: RF): -66 dB

Signal: coherent background: > 10 dB

Signal: noise (10 mW input): > 30 dB

Notes:

(a) Abbreviations are:

LL = round trip time in the sapphire rod for longitudinal waves.

LS = round trip time in sapphire rod for echo which propagates longitudinally one way and as a shear wave in the other direction.

LLLL = time for two round trips of longitudinal waves in sapphire rod.

From the summary of pulse heights, we see that the nitrogen microscope operates at 2.6 GHz with relatively low insertion loss and good signal-to-noise ratio. Unlike the case in helium, the coherent background is much smaller than the information signal. Thus interference between the two signals is not a problem. The performance of the lens in liquid argon is found to be nearly identical to that in nitrogen.

D. IMAGES IN LIQUID NITROGEN AND LIQUID ARGON

A wide variety of objects have been imaged in the nitrogen/argon microscope. Among these are microelectronic components, biological preparations, as well as grating structures which serve to test the resolution of the microscope. A sampling of the images taken by the microscope is presented below. The frequency of operation of the microscope for these images ranges from 1.7 GHz to 2.6 GHz. A 30 μm radius lens with glass matching layer was used to take pictures at the lower frequencies. Liquid argon was the liquid primarily used because of the better impedance match to this glass-coated lens. The carbon-coated 18 μm radius lens described in Section C of this chapter was used to take pictures at the higher frequencies. Liquid nitrogen was the liquid most often used with this lens.

D.1. Resolution Test Objects

One way to evaluate the resolution of an imaging system is to observe the system's response to periodic structures. To check the resolution of the microscope operating in liquid argon, a grating with spatial period of 0.4 μm was imaged.[7] The grating is composed of lines

of photoresist which are 0.2 μm wide and 0.15 μm thick on a silicon wafer. Figure 3-3(a) shows an acoustic image of the grating taken in liquid argon at 2.0 GHz. The corresponding acoustic wavelength is 0.42 μm. The image in Fig. 3-3(a) shows that the grating is clearly resolved and is imaged with excellent contrast. It is believed that the variation in width of the lines in the image is due to real structure in the object.

Figure 3-3(b) shows a scanning electron micrograph of a different region of the photoresist grating. The SEM image, of course, shows resolution superior to the acoustic image. Figure 3-3(c) shows an optical image which was taken with a high power, dry objective. With both of these microscopic methods, it was necessary to coat the grating with a thin (≈ 500 Å) layer of gold. For SEM imaging this was necessary in order to prevent the build up of charge on the surface. In the optical case, the coating was necessary in order to enhance the contrast of the low reflectance, nearly transparent photoresist.

At 2.0 GHz the period of the grating is 0.95 λ. Because of the large opening angle of the acoustic lens, it is not surprising that a structure with sub-wavelength periodicity can be resolved. From imaging theory, the spatial frequency cut-off of a focused imaging system is given by[8]

$$\nu_c = \frac{1}{\lambda(f\#)} \tag{3.1}$$

where λ is the wavelength and $f^{\#}$ is the ratio of lens diameter to focal length. For a lens with 53° opening half-angle, $f^{\#} = 0.8$. Thus

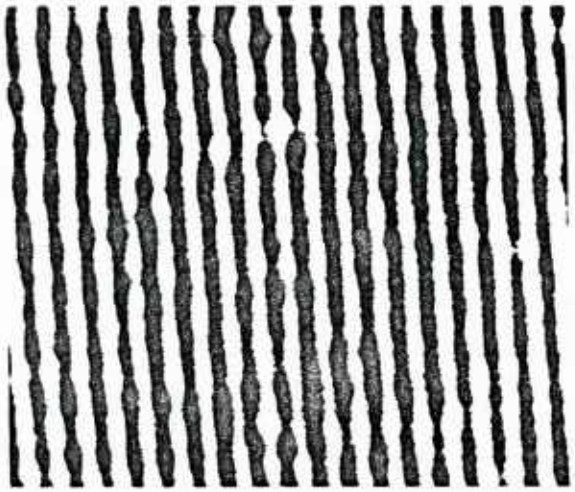

(a)

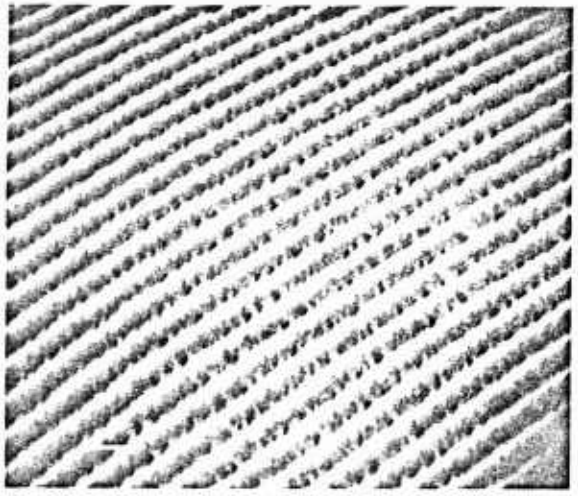

(b)

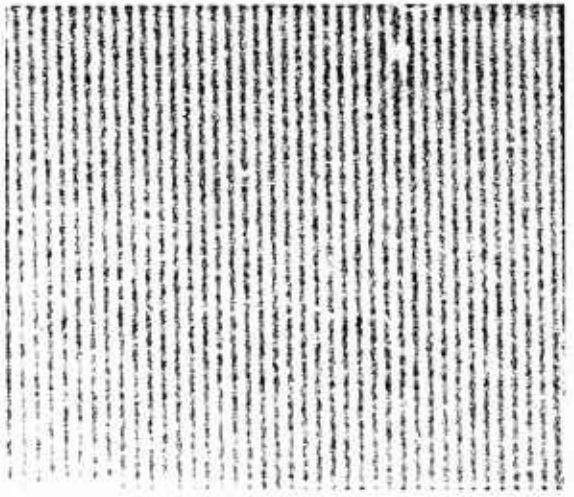

(c)

FIGURE 3.3--Images of grating with 4000 Å period. The acoustic image (a) was taken in liquid argon at 2.0 GHz. Images (b) and (c) are by scanning electron and optical microscopy, respectively.

the microscope should be able to resolve structures which have spatial period as small as 0.8 λ.

To find the spatial frequency cut-off of our lens, the operating frequency of the microscope was reduced until the grating was no longer visible. This occurred at approximately 1700 MHz. At this frequency, the grating period is approximately 0.8 λ. Thus we demonstrated that the acoustic lens is imaging with the theoretically expected performance.

D.2. Microelectronics

The acoustic microscope operating near room temperature has been demonstrated to have useful applications in the field of microelectronics. Many of these applications are inaccessible using other microscopic techniques. Bray[6] showed that the acoustic microscope can be used to detect regions of poor adhesion in evaporated metallic films on a substrate. Atalar[5] showed that contrast in images of integrated circuits is sensitive to the thickness and elastic properties of subsurface layers. Jipson[4] studied the correlation of certain features in acoustic micrographs with the presence of high leakage currents in MOS field effect transistors.

It is expected that many of these room temperature applications will be accessible to cryogenic acoustic microscopy as well. The cryogenic microscope offers several advantages over the water instrument in microelectronic applications. One advantage is the higher available resolution. As integrated circuit structures shrink in size, the cryogenic microscope may be the only means by which the elastic properties of submicron size structures can be probed with sufficient

resolution. Another advantage of cryogenic acoustic microscopy is the electrical and chemical inertness of the liquid medium. It is well known that water has a high dielectric constant ($\varepsilon = 78$) , can be electrically conductive and is corrosive to many materials. The cryogenic liquids, on the other hand, have low dielectric constant ($\varepsilon = 1.5$ for nitrogen and argon), are electrically insulating and are chemically inert. These factors are important especially if experiments with electrically active circuits are of interest. To be fair, it must be noted that the electrical characteristics of most semiconductor devices change significantly upon cooling to cryogenic temperatures.

As an initial application of the nitrogen/argon microscope to the field of micro-electronics, we imaged a dual-gate gallium-arsenide microwave field effect transistor.[9] Figures 3-4(a) and (b) show acoustic images of the device taken at two slightly different focal positions. The operating frequency was 2.0 GHz. An optical micrograph taken with a high power (100 X, N.A. = 1.25) oil immersion objective is shown in Fig. 3-4(c) for comparison. The two horizontal parallel structures are metallic gates. The gate widths are approximately 1 μm. We note that the acoustic images show good contrast and that the gates are easily resolved. The change in contrast which acompanies the change in focal positions [compare Fig. 3-4(a) with (b)] is similar to the $V(z)$ effects that are encountered in water microscopy of integrated circuits.

As an example of a diagnostic application of cryogenic acoustic microscopy, we show another microwave FET in Fig. 3-5(a). This device is similar to the previous one except that it has only one gate element. In the metallization connecting the gate to its bond pad, we

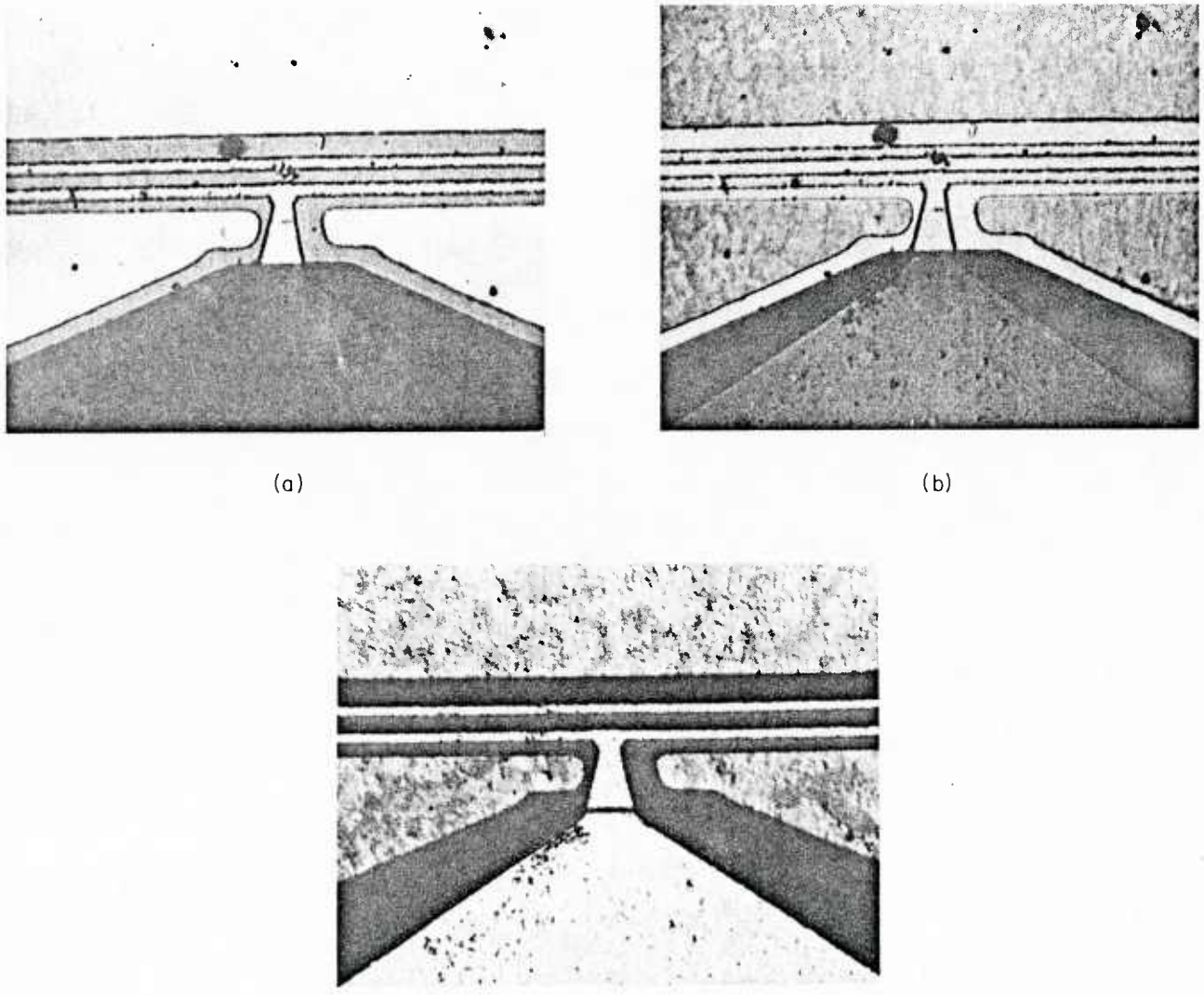

(a)

(b)

(c)

FIGURE 3.4--Images of dual gate GaAs field effect transistor. Images (a) and (b) are acoustic and taken at two different focal positions. Image (c) is by optical oil-immersion differential interference contrast.

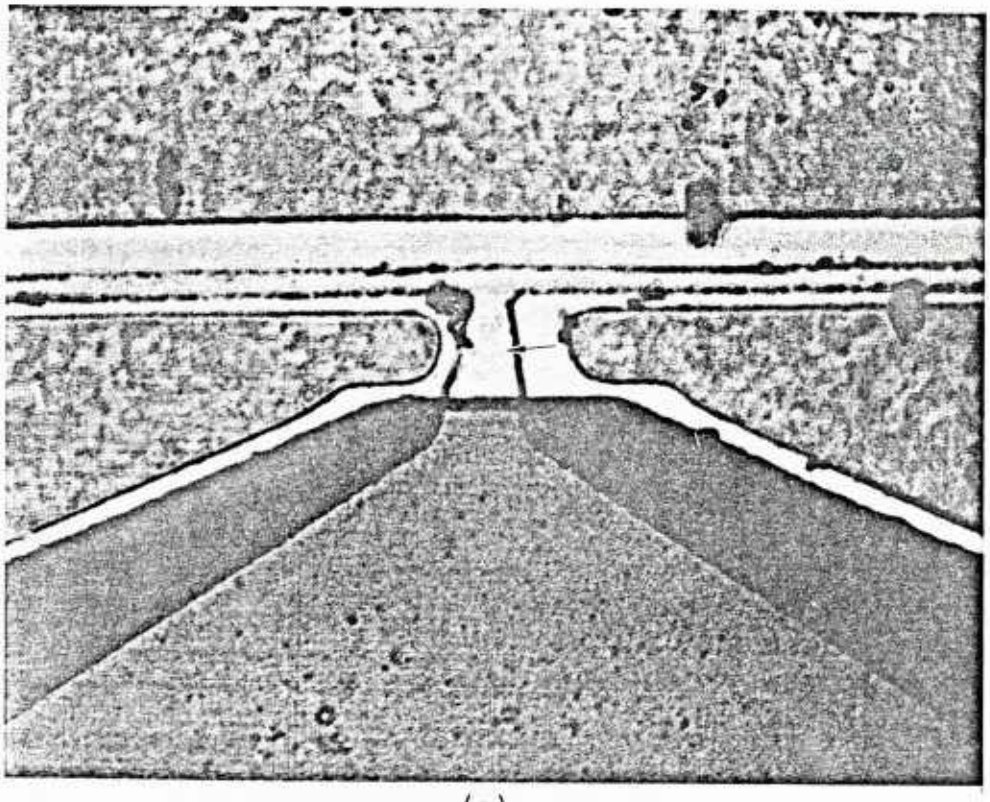

(a)

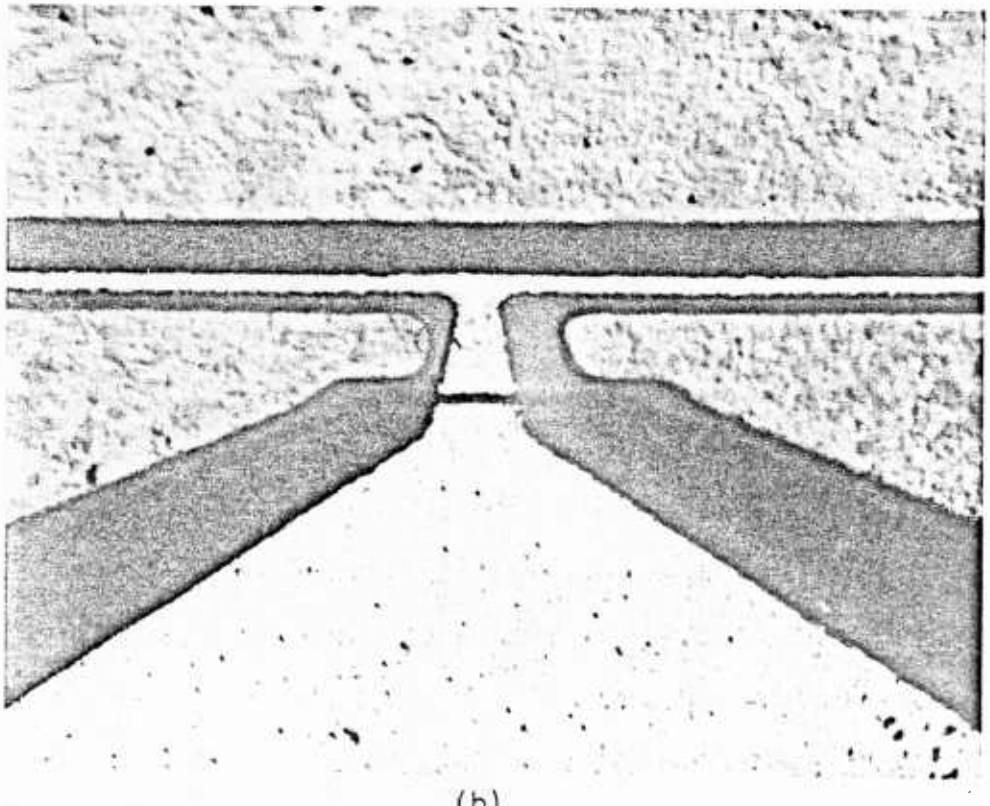

(b)

FIGURE 3.5-Images of single gate GaAs FET. Image (a) is acoustic and the arrow points to a region of anomalous acoustic contrast. Image (b) is by optical oil-immersion DIC.

see a region where the contrast abruptly changes. This is indicated by the arrow in the figure. This feature may be associated with defective metallization. The same feature can be seen only faintly in the optical image of Fig. 3-5(b).

REFERENCES FOR Section 3

1. N.B. Vargaftik, Tables on the Thermophysical Properties of Liquids and Gases in Normal and Dissociated States (Hemisphere Pub., Washington, 1975).
2. R.B. Lindsay, in American Institute of Physics Handbook, D.E. Gray, Ed. (McGraw-Hill, New York, 1972), p. 2-161.
3. R.A. Lemons, "Acoustic Microscopy by Mechanical Scanning," Ph.D. Dissertation, Stanford University (1975).
4. V.B. Jipson, "Acoustic Microscopy at Optical Wavelengths," Ph.D. Dissertation, Stanford University (1979).
5. A. Atalar, "Acoustic Reflection Microscope," Ph.D. Dissertation, Stanford University (1978).
6. R.C. Bray, "Acoustic and Photoacoustic Microscopy," Ph.D. Dissertation, Stanford University (1981).
7. The grating is courtesy of IBM Corporation.
8. W.J. Smith, in Handbook of Optics, W.G. Driscoll and W. Vaughn, Eds. (McGraw-Hill, New York, 1978).
9. Courtesy of Hewlett-Packard Corporation.

4. IMAGING WITH THE MICROSCOPE

The first acoustic images in helium were taken at a temperature of 1.95 K and a sound frequency of 630 MHz.[1] The temperature corresponds to a local minimum in the sound attenuation (which is quite large) and was achieved using a pumped helium bath in a simple cryostat. The results were impressive enough to warrant the more complicated and expensive dilution refrigerator required to realize the full potential of helium for acoustic microscopy.

A. IMAGING

The operating frequency of the very low temperature helium microscope began at 980 MHz.[2] The acoustic wavelength in helium was 2400 Å. None of the improvements of the signal-to-noise ratio discussed in section 2 were implemented, and the imaging was poor due to nonlinearity. Figure 4.1 shows two images taken at $T = 0.1$ K. The object is a 4 μm period grating consisting of 1000 Å thick aluminum lines on glass. Many small dirt-like particles can be seen in both images. These particles are believed to be frozen air which have selectively condensed onto the aluminum grating lines. The resolution of the imaging appears to be 4000 Å to 5000 Å which is consistent with the expected lateral resolution of $F\lambda = 4560$ Å, where F is the F-number of the lens, equal to 1.9 in this case. The signal-to-noise ratio for these images was approximately 5 dB.

IMAGING IN HELIUM

T = 0.1°K, F = 980 MHz, λ = 2400 Å

(a)

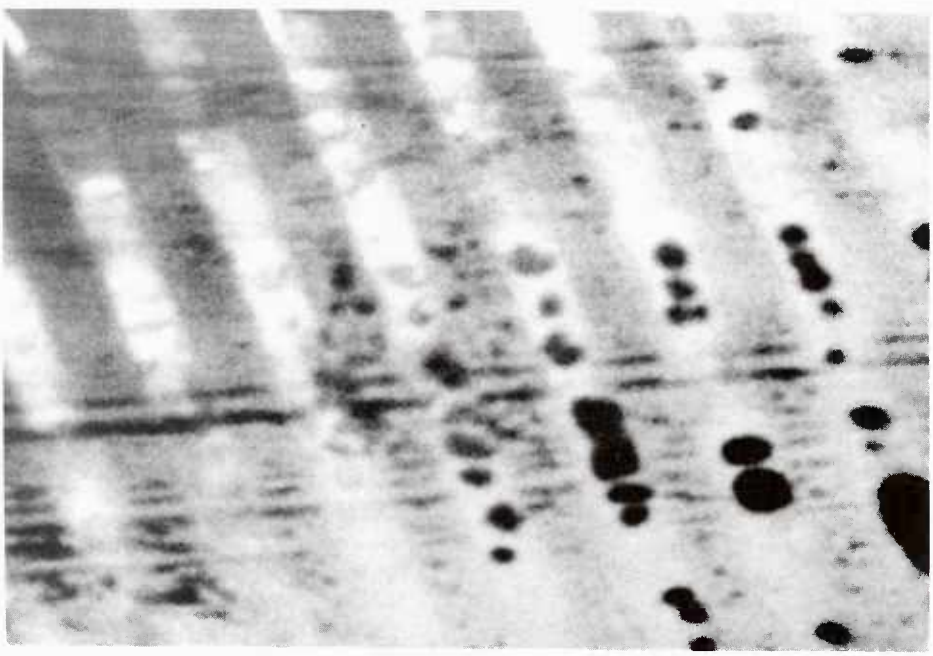

(b)

FIGURE 4.1--Images taken in liquid helium at approximately 0.05°K. The object is a 4 μm period grating consisting of aluminum lines on glass. Bar = 4 μm.

To improve both the signal-to-noise ratio and resolution, the microscope was modified to operate at 2.6 GHz with the helium-cooled low noise microwave amplifiers discussed in section 2. The results are shown in Figs. 4.2 and 4.3. The object is a 2 μm period grating of 1000 Å-thick aluminum lines on glass. The aluminum strips are slightly wider than the bare glass. A great amount of structure can be seen on the glass, including islands of aluminum separate from the main strips. The acoustic wavelength in helium at 2.6 GHz is about 900 Å, and with the f/.8 aperture lens used (F-number equal to 1.8, we expect a resolution of less than 800 Å, which was achieved.

The lens assemblies used at 980 MHz and 2.6 GHz were taken directly from water acoustic microscopes; that is they were designed for use in water. When a similar lens designed for 4.2 GHz in water was used in helium, no return signal from the sample could be found and no images could be recorded. The problem was that the design criteria for all the parameters of the acoustic lens (length, lens aperture, lens radius, transducer radius) operating in water do not work well in helium. Because helium has negligible acoustic attenuation, the lens can be large. This allows more working distance in helium than would be allowed in water. Also, the blank length can be much longer, and the lens' radius can be chosen so that the timing of the signal echo is directly in between two of the acoustic rattles within the sapphire. Proper positioning of the signal echo timing allows narrower bandwidth detection of the signal and therefore lower noise in the receiving system.

IMAGING IN HELIUM

T = 0.2 °K, F = 2.6 GHz, λ = 900 Å

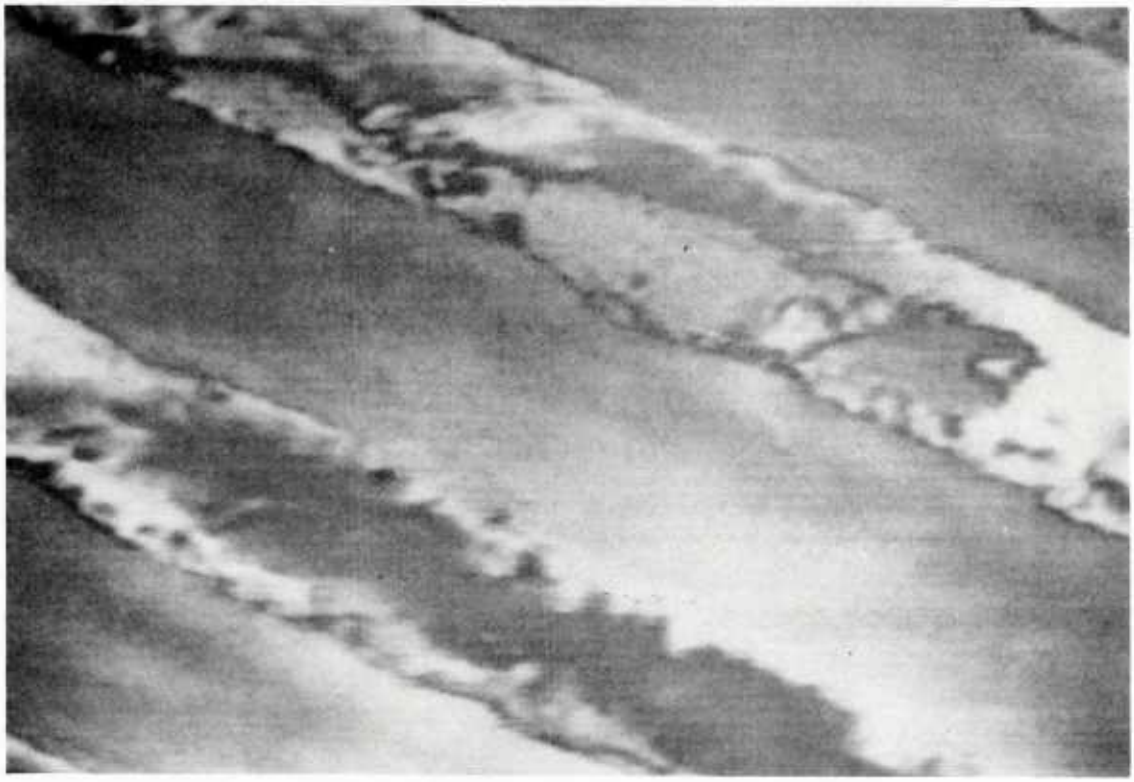

FIGURE 4.2

IMAGING IN HELIUM

T=0.2 °K, F=2.6 GHz, λ=900 Å

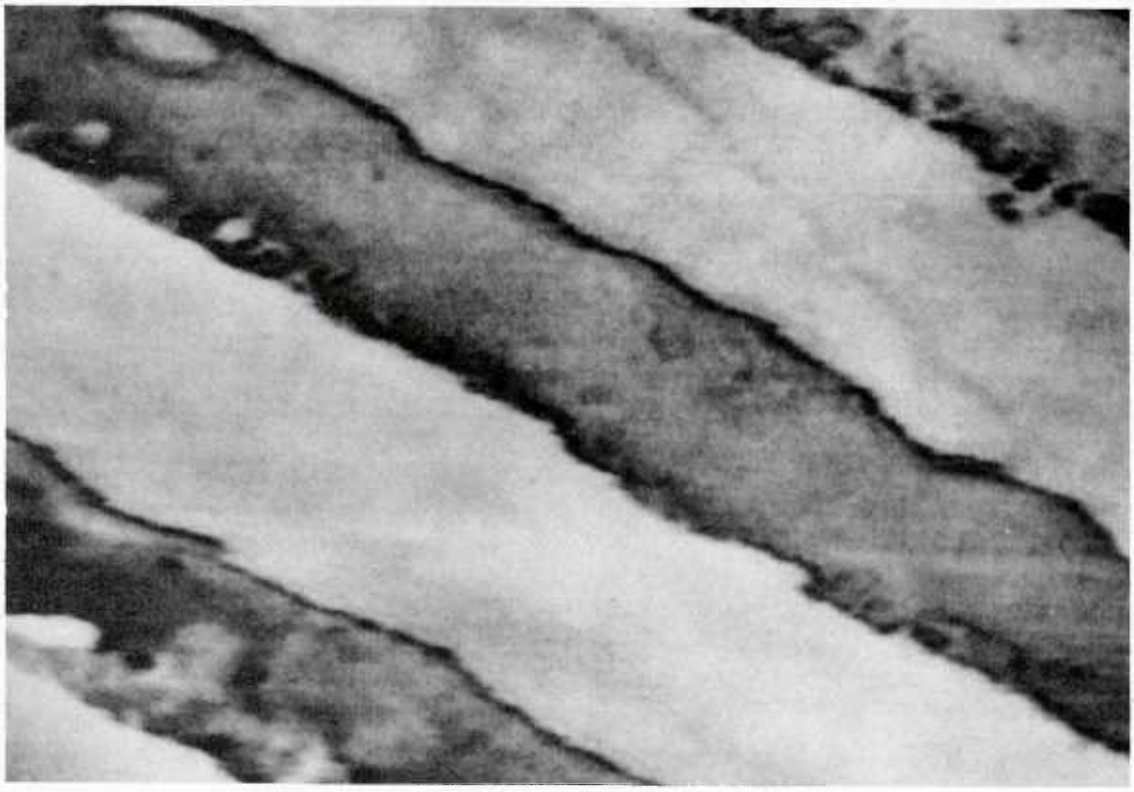

FIGURE 4.3

Because of the acoustical saturation properties of the helium, a lens must be designed so that the transducer most efficiently receives the sound waves from a completely illuminated lens. Earlier water lenses were designed so that the transducer properly illuminated the lens;[3,4] however, the saturation effect always allows good illumination of the lens. For example, if the edge of the lens is poorly illuminated and the acoustic power 10 dB weaker than the center, the input power need only to be increased 10 dB past the saturation level to ensure uniform illumination. Hence, one must only consider the illumination of the transducer by the lens for the return path. When this concept is combined with those of the last paragraph, a lens suitable for the helium microscope can be designed. The following lists some of the characteristics of a lens designed for use at 4.2 GHz. Note the large lens size (4 times a typical water lens at this frequency) and that the transducer is roughly the same size as the lens aperture diameter, whereas the transducer is usually two to three times larger for use in water.

Operating frequency: 4.2 GHz

Wavelength in helium: 566 Å

Material: sapphire

Lens radius: 86 μm

Lens opening half-angle: 57°

Rod length: 2650 μm

Rod diameter: 0.25 inch

Matching layer: Amorphous Carbon[3]

Transducer radius: 86 μm

Conversion efficiency: -10 dB

Lens Illumination loss: 0.7 dB

Pulse timing:

RF to LL: 476 ns

RF to LLLL: 952 ns

RF to signal: 1199ns

RF to LLLLLL: 1428 ns

where RF is the timing of the initial microwave pulse applied to the transducer, LL is the round trip time in the sapphire rod for the longitudinal waves, LLLL is two round trips, etc.

The lens assembly designed for 4.2 GHz operation in helium was the first which could not be tested using water as the acoustic coupling media between the lens and a sample. The lens was installed directly into the dilution refrigerator along with two-stage cooled pre-amplifiers designed for 4.2 GHz. Some of the results are shown in Figs. 4.4 through 4.7, demonstrating high quality imaging with a 20 dB signal-to-noise ratio and a lateral resolution of less than 500 Å.

Figures 4.4(a) and 4.4(b) demonstrate individual acoustic images taken in helium at a temperature less than 0.1 K. The object is a bipolar transistor on a silicon integrated circuit.[5] Visible in the images are 2 μm-wide, 0.5 μm-thick aluminum lines making connections to the emitter and base of the transistor. Figure 4.4(a) was recorded with the silicon substrate in the focal plane of the acoustic lens, while Fig. 4.4(b) was recorded with the aluminum lines in focus.

The superfluid helium acoustic microscope exhibits a very narrow depth of focus. At 4.2 GHz, the depth of focus is approximately

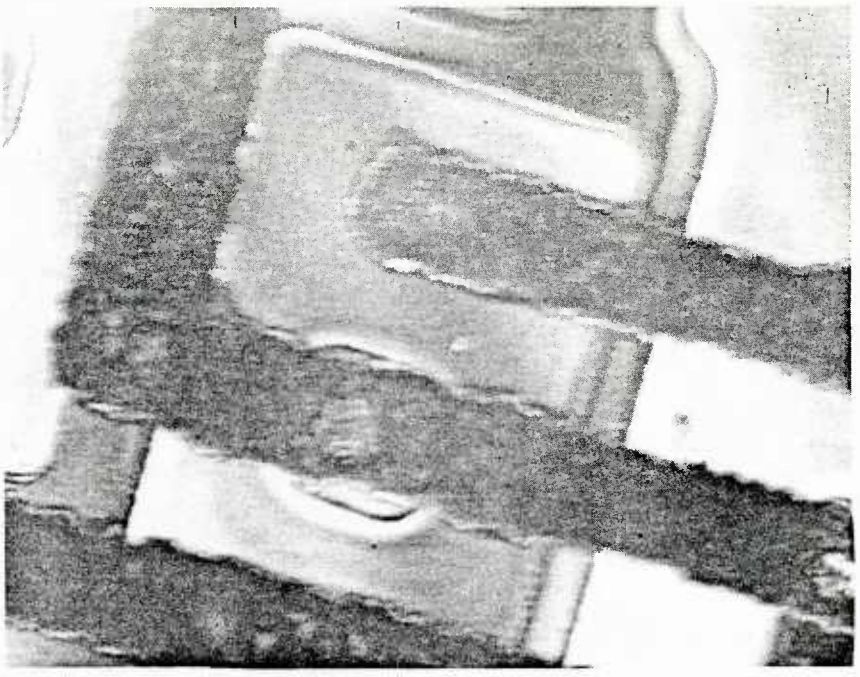

(a)

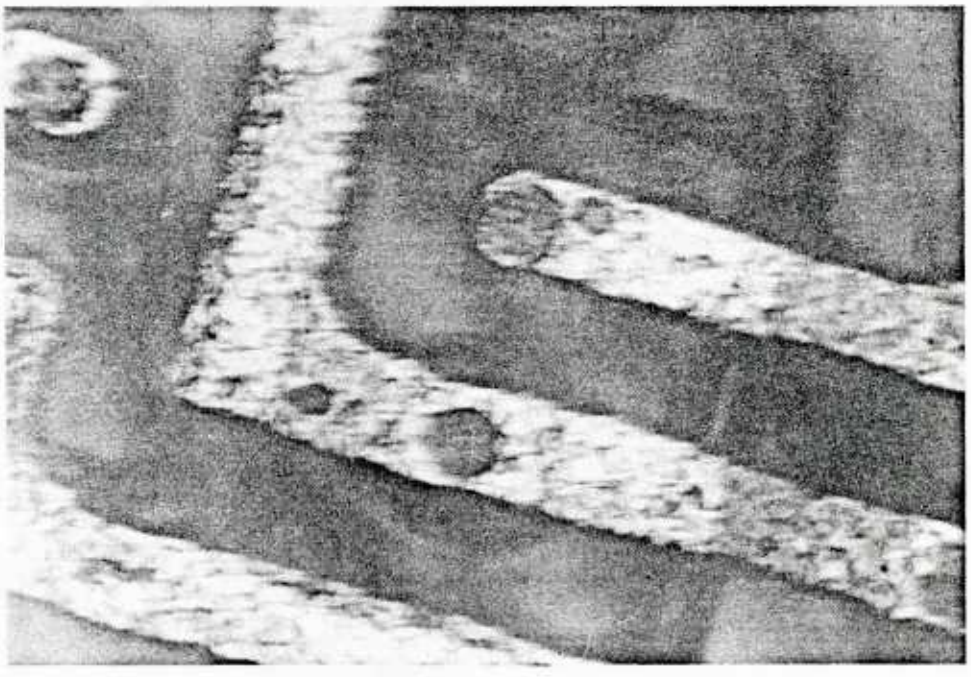

(b)

FIGURE 4.4--Bipolar transistor imaged at 4.2 GHz.

1300 A. Because of this and the considerable vertical relief on the integrated circuit, it is not possible for the silicon substrate and the top surface of the aluminum lines to be in focus simultaneously. To present information from both the substrate and the aluminum lines in a single picture, the images in Fig. 4.4 have been digitally stored and superposed electronically to form the composite micrograph in Fig. 4.5(a). For display purposes, one can assign different colors to each focal plane image and show the composite result on a color monitor; however, color images are not shown here.

Figure 4.5(b) is a Scanning Electron Microscope (SEM) image of the same bipolar transistor shown in the acoustic image of Fig. 4.4(a). The SEM has a very long depth of focus and thus can be considered a complementary tool to the helium acoustic microscope. This is augmented by the fact that electron and acoustic microscopes have very different contrast mechanisms. The helium acoustic microscope's contrast mechanisms will be discussed later in this chapter.

Figures 4.6(a) and (b) shows a high magnification view of the aluminum line connection to the emitter of the same bipolar transistor displayed in Figs. 4.4 and 4.5. Figure 4.6(a) is an acoustic image and Fig. 4.6(b) is a SEM image shown for comparison. Considerable detail is evident in the acoustic image which probably reflects the grain structure of the aluminum. The acoustic features are thought to arise only from topographical changes. The SEM image shows less contrast and indicates the instrument's insensitivity to small height changes in the sample.

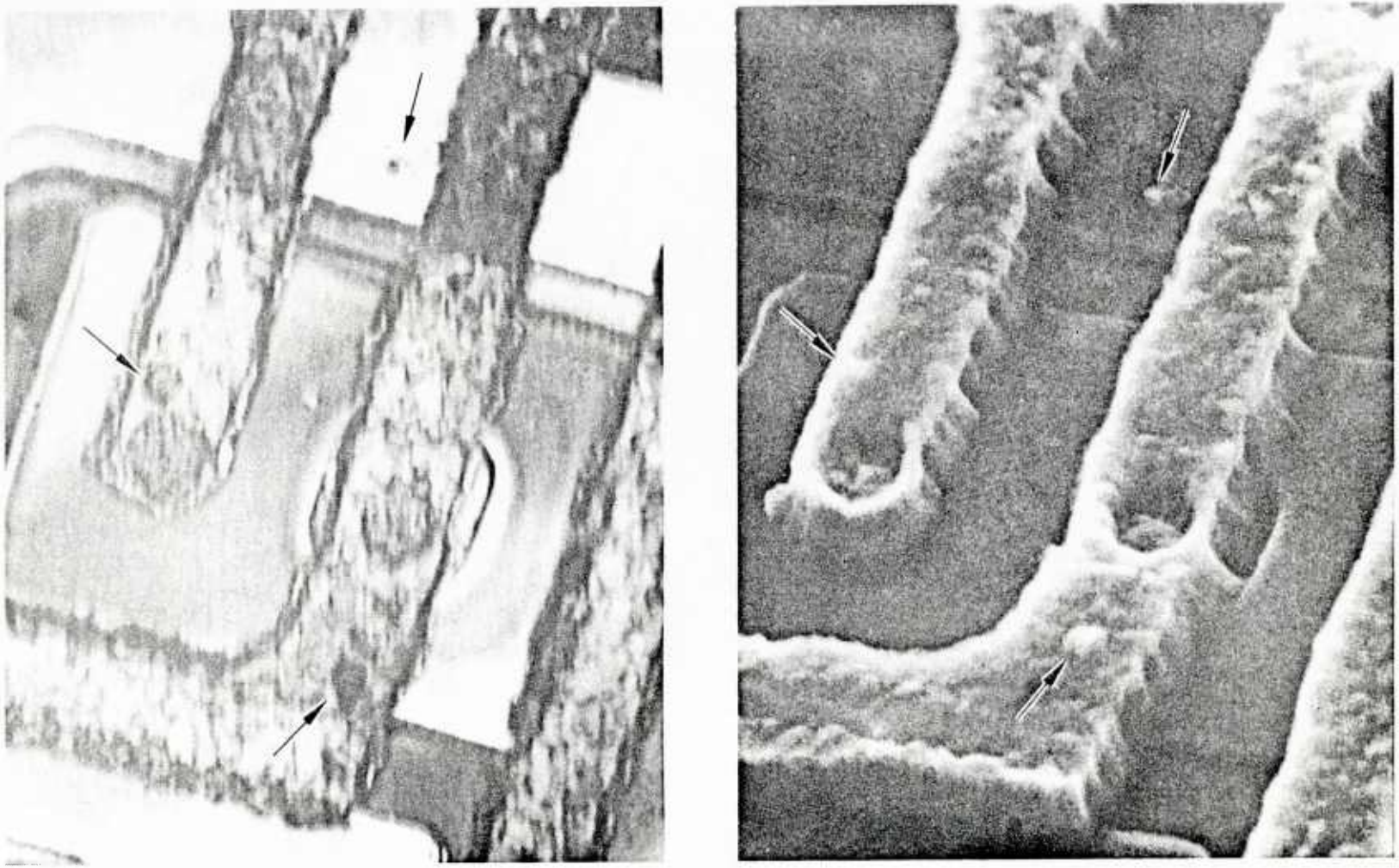

(a) (b)

FIGURE 4.5--Bipolar transistor.

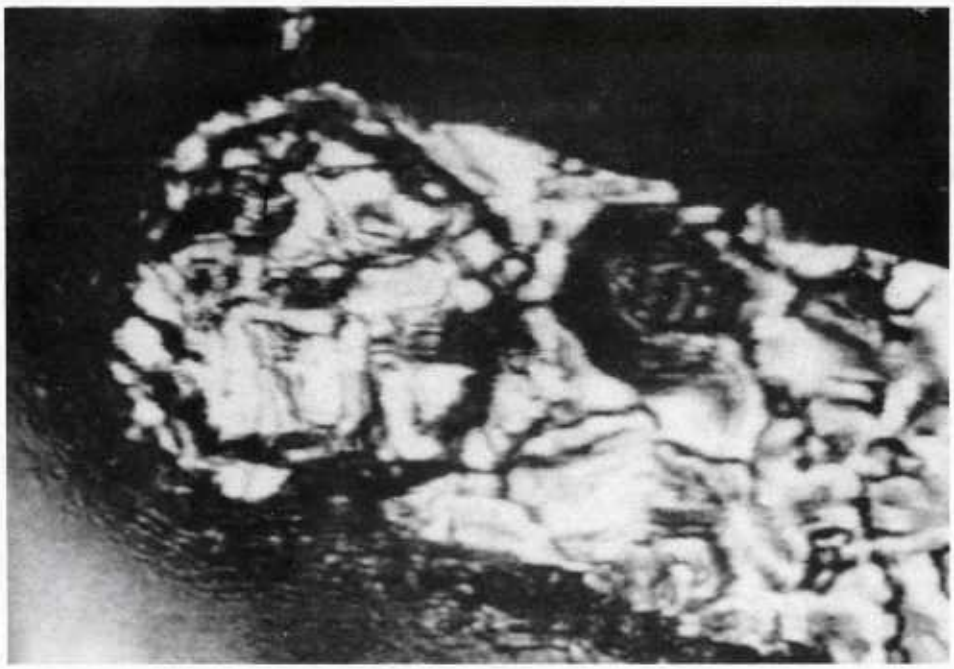

(a) ACOUSTIC

(b) SEM

FIGURE 4.6--Aluminum line on the emitter of a bipolar transistor.

Finally, Fig. 4.7 shows another high magnification image of an aluminum line, this time at a base contact of a transistor. Again, features resembling grain boundaries are visible. The operating frequency of the microscope for Figs. 4.4 - 4.7 was 4.2 GHz and the sound wavelength in the helium was 566 Å. We expect, and indeed obtain, resolution better than 500 Å in these images, indicating that the microscope exhibits a diffraction limited focus. A determination of find a spatial frequency cut-off, giving the lateral resolution of the microscope.[6] For our small dimensions, however, such gratings are not readily available. We simply note that there are structures visible in Fig. 4.7 with a full linewidth as narrow as 300 Å.

To improve the resolution of the acoustic microscope further, the operational frequency was extended to 8.0 GHz. If no improvements had been made to the microscope system, the signal-to-noise ratio would have decreased significantly for several reasons. Doubling the frequency from 4 GHz to 8 GHz decreases the saturating input power by 6 dB (see section 2, Section B). The noise temperature of the pre-amplifiers increases by 2-3 dB.[7] There is also an increase in the insertion loss of the acoustic transducers as the frequency is raised.[8] Considering all the effects described above, there is at least a 15 dB decrease in the signal-to-noise ratio when the frequency is raised from 4.2 GHz to 8.0 GHz. To offset this problem, the microscope system was altered to make use of pulse expansion and compression techniques (chirp) (see section 2). Operation at 8 GHz now features a signal-to-noise ratio of 15 dB using 300 Å acoustic waves for imaging. The lateral resolution is 200 Å and has been demonstrated with both biological and integrated circuit samples.[8]

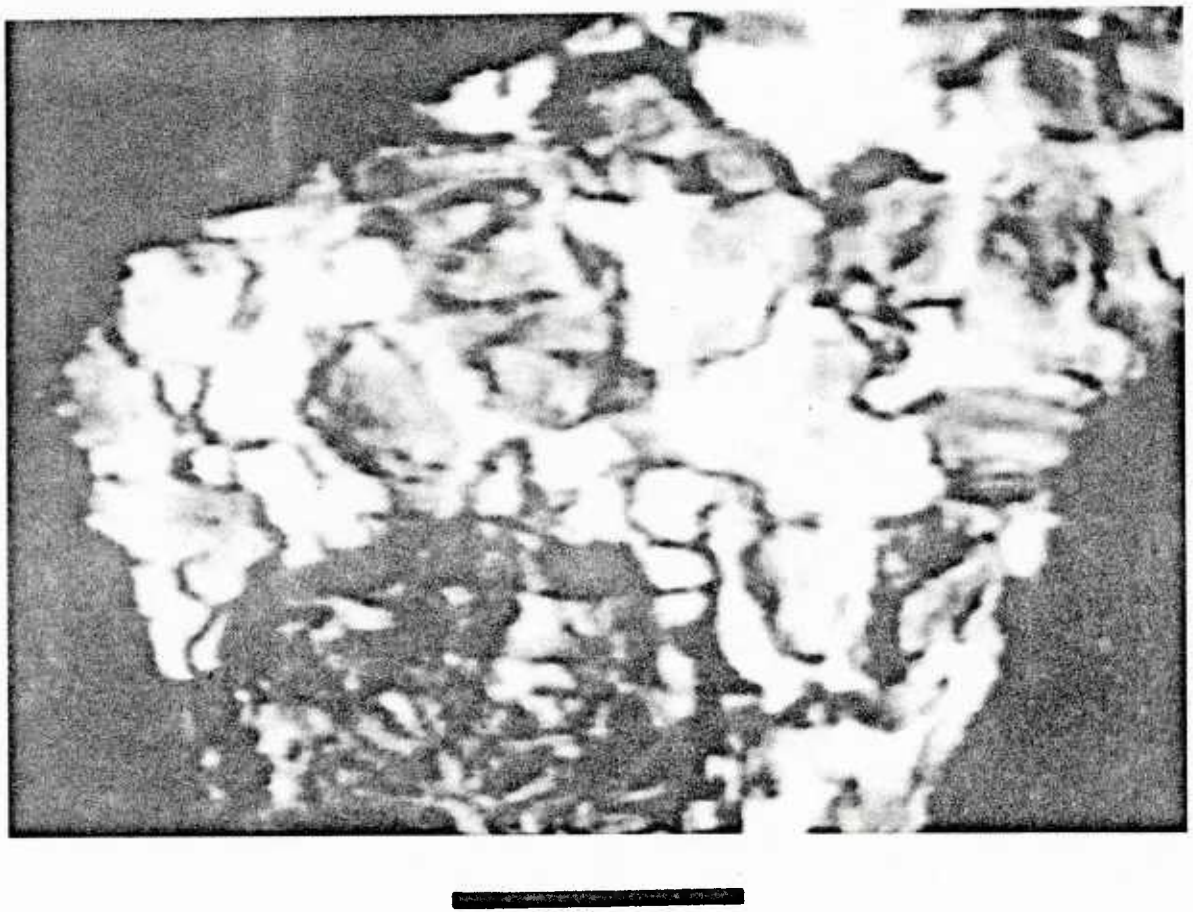

FIGURE 4.7--Aluminum line on the base of a bipolar transistor imaged at 4.2 GHz.

Figures 4.8(a) and (b) show an 8.0 GHz acoustic image and an SEM micrograph of similar regions of a 2 μm wide polysilicon line on a CMOS integrated circuit.[8,9] Crystal grain structure can easily be seen in the acoustic image. The details in the acoustic image indicate that the resolution of the acoustic microscope is about 200 Å, which means the focus must be diffraction limited. Crystal grain structure can easily be seen in the acoustic image. However, when the integrated circuit was imaged directly by the SEM, the polysilicon line showed no structure whatsoever, even at an electron voltage of 30 kV. The sample was then coated with a 100 Å thick layer of gold-palladium, and the structure seen in Fig. 4.8(b) appeared only at a high electron voltage of 30 kV.

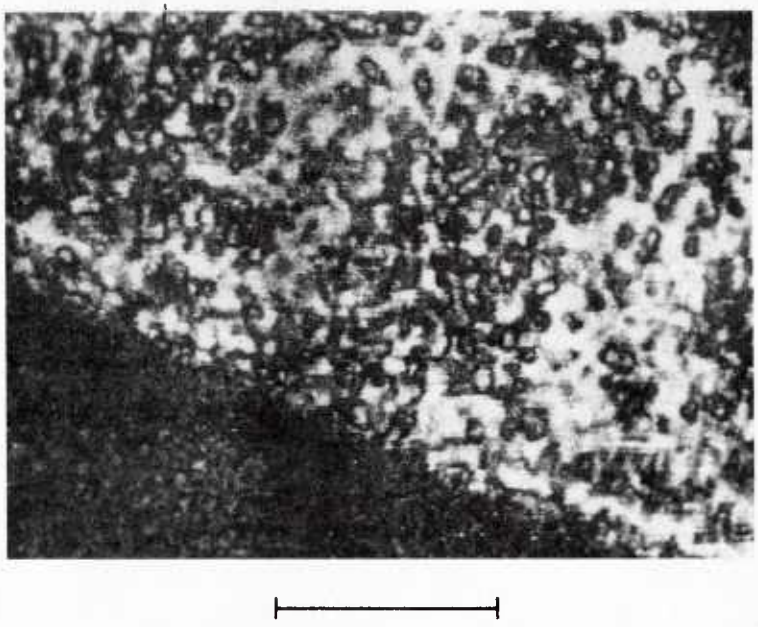

(a)

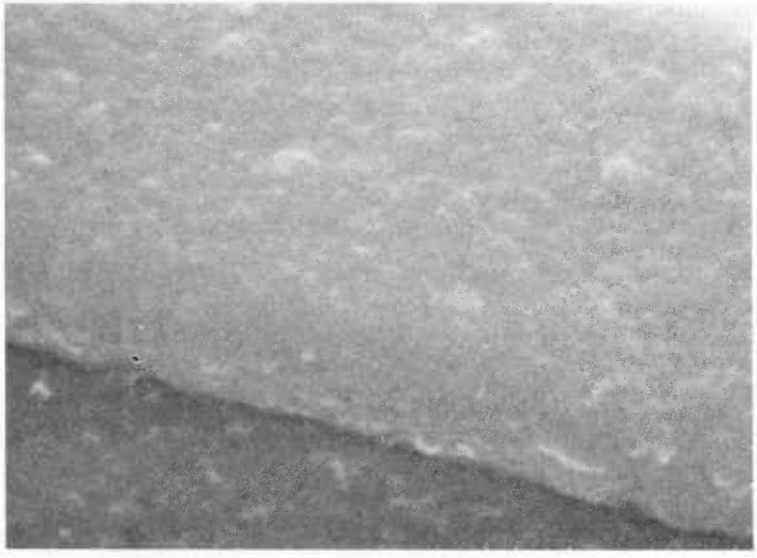

(b)

FIGURE 4.8--(a) Acoustic and (b) SEM micrographs of similar regions of a polysilicon line on a CMOS integrated circuit. Scale bars are 1 μm.

REFERENCES FOR SECTION 4

1. J. Heiserman, D. Rugar, and C.F. Quate, J. Acoust. Soc. Am. 67, No. 5, 1629 (1980).
2. D. Rugar, J.S. Foster, and J. Heiserman, Acoustical Imaging, E.A. Ash and C.R. Hill, Eds. (Plenum Press, New York, 1982), pp. 13-25.
3. V.B. Jipson, Ph.D. Dissertation, Stanford University (1979).
4. D. Rugar, Ph.D. Dissertation, Stanford University (1981).
5. J.S. Foster and D. Rugar, Appl. Phys. Lett. 42, No. 10, 869 (1983).
6. J.W. Goodman, Introduction to Fourier Optics (McGraw-Hill, New York, 1968), pp. 110-113.
7. S. Weinreb, IEEE Trans. Microwave Theory Tech. 28, 1041 (1980).
8. B. Hadimioglu and J.S. Foster, submitted to J. Appl. Phys.
9. Courtesy of TRW Corporation.

5. IMAGING WITH HIGH INTENSITY FOCUSED BEAMS

A. INTRODUCTION

The intensity of acoustic waves in the focal region of an acoustic lens can exceed 10^4 W/cm^2. At these high intensities the propagation of acoustic waves in liquids is, in general, not adequately described by linear theories. This section discusses theory and applications of imaging with high intensity focused beams. In particular, it is demonstrated that under some circumstances the use of high intensity waves can significantly improve the resolution performance of the reflection acoustic microscope.

The high intensities available in the acoustic microscope have been used by earlier investigators to do a variety of nonlinear imaging experiments. Lemons[1] used a transmission mode microscope to produce images using second harmonic generation. In his experiments the transmitting lens of the microscope generated a focused beam at the fundamental frequency, ω_1. The receiver lens, confocal with the transmitting lens and tuned to $2\omega_1$, was then used to detect the second harmonic radiation which is generated in the object and in the coupling fluid. Lemons found that a large proportion of the second harmonic generation came from the coupling medium rather than the object. Since this situation was considered undesirable, other geometries were considered in order to emphasize the nonlinear behavior of the object. To this end, Yeack[2] constructed a three lens acoustic microscope which used three-wave mixing for imaging. In the three wave mixing

experiments, two lenses generate focused acoustic beams at frequencies ω_1 and ω_2. The focused beams are oriented at right angles to one another and overlap only in the focal region. This geometry ensures that the nonlinear interaction is confined to the close proximity of the focus. A third lens which serves as the receiver is tuned to the frequency of a mixing product, either $\omega_1 + \omega_2$ or $\omega_1 - \omega_2$. Despite considerable experimental complexity, images of spatially distributed nonlinear response in PVF_2 and in mica bearing granite samples were obtained.

In many ways the nonlinear imaging experiments described in this chapter are simpler than those done by Lemons or Yeack. The emphasis of this study is the effect that harmonic generation in the liquid has on the imaging properties of the microscope. A microscope with a single acoustic lens is used and only a single frequency, the fundamental, is transmitted and received. The nonlinear response in these experiments is observed by monitoring the effect that harmonic generation has on the strength of the received fundamental frequency. In order for resolution improvement to be observed, the intensity of the fundamental must be high enough so that a significant fraction of its power is converted into harmonics. Some of the experiments described in this section are performed with a fundamental wave that has been depleted by over 90%.

The section is organized in the following way. Section B presents an introductory discussion of finite amplitude plane wave propagation in nonlinear media. In particular, the nonlinear behavior of water and liquid nitrogen is compared. Section C presents experimental results of operating the acoustic microscope at high power levels in liquid nitrogen and water. Particular attention is given to the depletion of

the fundamental and to the resulting improvement in imaging resolution. Section D outlines a simple physical model which shows how energy in the harmonics can be transferred back to the fundamental wave after passage through the focal region.

B. FUNDAMENTALS OF NONLINEAR ACOUSTICS

The propagation of acoustic waves in classical fluids is governed by the equations of hydrodynamics. If the propagation is assumed to be free of dissipation, the Euler equations provide the basis of the acoustic equations. If viscous and heat conduction losses are included in the analysis, the Navier-Stokes equations must be used. The equations are[3,4]

$$\frac{d\rho}{dt} + \rho\nabla \quad \vec{v} \quad = \quad 0 \qquad (5.1a)$$

$$\rho \frac{d\vec{v}}{dt} = -\nabla p + \eta \nabla^2 \vec{v}$$

$$+ (\zeta + \eta/3)\, \nabla(\nabla \quad \vec{v}) \tag{5.1b}$$

$$\rho T \frac{ds}{dt} = \nabla \quad (\kappa \nabla T) + Q \tag{5.1c}$$

$$p = p(\rho, s) \tag{5.1d}$$

where ρ is the fluid density, $\vec{v}$ the fluid particle velocity, p the pressure, η the shear viscosity, ζ the bulk viscosity, s the entropy per unit mass, T the temperature and κ the thermal conductivity. The convective derivative is given by

$$\frac{d}{dt} = \frac{\partial}{\partial t} + \vec{v} \quad \nabla$$

The first equation of the set presented above is the continuity equation. The second equation is Newton's second law describing the forces acting on the fluid. The third equation is the heat flow equation. The term Q in this equation is a term accounting for viscous heating of the liquid. The last equation is the equation of the state of the fluid.

The equation of state of the liquid is often expanded in a power series about its equilibrium state. The first few terms of the series for an isentropic equation of state are

$$p = p_o + \left(\frac{\partial p}{\partial \rho}\right)_{\rho_o, s} (\rho - \rho_o) + \frac{1}{2}\left(\frac{\partial^2 p}{\partial \rho^2}\right)_{\rho_o, s} (\rho - \rho_o)^2 + \cdots ,$$

or

$$p = p_o + A\left(\frac{\rho - \rho_o}{\rho_o}\right) + \frac{B}{2}\left(\frac{\rho - \rho_o}{\rho_o}\right)^2 + \cdots , \qquad (5.2)$$

where

$$A = \rho_o \left(\frac{\partial p}{\partial \rho}\right)_{s, \rho_o} \qquad (5.3)$$

$$B = \rho_o^2 \left(\frac{\partial^2 p}{\partial \rho^2}\right)_{s, \rho_o} . \qquad (5.4)$$

B.1 Linear Acoustics

To obtain the linear acoustic wave equation, the equations in (5.1) are linearized by writing

$$\rho = \rho_o + \rho' \qquad (5.5)$$

$$p = p_o + p' , \text{ etc.}$$

The 'primed' variables represent small variations from equilibrium values. Equations (5.5) are substituted into the Navier-Stokes

equations and all terms higher than first order in the primed variables are neglected.

The linearized equations result in the wave equation

$$\left(\nabla^2 - \frac{1}{C_o^2}\frac{\partial^2}{\partial t^2}\right)\rho' = -\frac{D}{C_o^4}\frac{\partial^3 \rho'}{\partial t^3} \tag{5.6}$$

where C_o, the speed of sound, is given by

$$C_o^2 = A/\rho_o = \left(\frac{\partial p}{\partial \rho}\right)_{\rho_o, s}$$

and D, the acoustic diffusivity, is defined by

$$D = \left(\frac{4}{3}\eta + \zeta\right) + \left(\frac{1}{C_v} - \frac{1}{C_p}\right)\kappa$$

where C_v is the specific heat at constant volume and C_p is the specific heat at constant pressure. The term on the right side of (5.6) is the acoustic loss term.

It is easy to show that one possible solution of (5.6) is the attenuated plane wave solution

$$\rho'(z,t) = \mathrm{Re}\left[\rho_o' e^{-\alpha z} e^{i(kz-\omega t)}\right] ,$$

where $k = \omega/c$,

$$\alpha = \frac{1}{2}\frac{\omega^2}{C_o^3} D \tag{5.7}$$

and ρ_o' is a complex constant chosen to satisfy the boundary condition

at $z = 0$. In arriving at this solution it was assumed that $k >> \alpha$. This is true in cases of interest to us.

B.2 Nonlinear Acoustics -- Plane Waves

The linear wave equation (5.6) is valid only for acoustic waves of infinitesimal strength. We now consider the more difficult case of finite amplitude acoustic waves. This subject has a long history and we will only review some of the results for the propagation of plane waves here.[5-8]

It is found both experimentally and theoretically that pressure peaks of finite amplitude waves propagate faster than the pressure troughs. This causes a wave which is initially sinusoidal to distort as it propagates. Such a wave will approach the shape of a sawtooth wave in the limit of high amplitude or, if there is no loss, long propagation distance. The importance of such nonlinear effects is governed by the size of the particle velocity relative to the speed of sound (the acoustic Mach number), the nonlinearity of the equation of state, the distance over which the sound travels and the acoustic attenuation of the liquid.

An important length scale in nonlinear acoustics is the discontinuity length. This is the distance at which, in the absence of attenuation, the slope of a portion of the waveform becomes infinite. The discontinuity length is given by

$$L = \left[(1 + B/2A) \frac{\omega v_o}{c_o^2} \right]^{-1} = \frac{1}{\beta M k} \qquad (5.8a)$$

where $\omega = 2\pi f$ is the angular frequency, v_o is the peak particle

velocity, $k = \omega/C_o$, $M = v_o/C_o$ is the acoustic Mach number and $\beta = (1 + B/2A)$.

The quantity B/A is the ratio of the two coefficients in the equation of state (5.2). The value of this ratio depends on the physical properties of the liquid. For water at 60°C, $B/A = 5.7$.[7] For liquid nitrogen at its normal boiling point, $B/A = 6.6$.[7]

To convert from acoustic intensity to an acoustic Mach number, the following relation is useful

$$I = \frac{1}{2} Z v_o^2 \quad , \tag{5.8b}$$

where I is the acoustic intensity (power per unit area) and $Z = \rho_o C_o$ is the acoustic impedance. We may then write

$$M = v_o/C_o = (2I/Z)^{1/2}/C_o$$

$$= \left(\frac{2\ I}{\rho_o C_o^3} \right)^{1/2}$$

Thus we see that high acoustic Mach numbers are more easily generated in media with low acoustic velocity and low acoustic impedance. This is an important point since cryogenic liquids have these properties.

Table 5-1 gives the Mach number and discontinuity length for liquid nitrogen and water at several different acoustic power levels. At 1000 W/cm^2 in water the Mach number is 0.002. For the same power level, liquid nitrogen has the value $M = 0.006$. This value is higher than in water because of the lower acoustic impedance and propagation velocity of nitrogen.

TABLE 5-1

Nonlinear Plane Wave Propagation in Water and Liquid Nitrogen

H_2O (60°C)

B/A = 5.7 f = 2.6 GHz

λ = 0.60 μm $1/\alpha$ = 13 μm

$I(W/cm^2)$	M	L	Γ	Excess Attenuation *
100	0.0007	34 μm	0.38	0 dB
1000	0.0023	11 μm	1.2	0.3 dB
10,000	0.0073	3.4 μm	3.8	3 dB
100,000	0.023	1.1 μm	12	10 dB

LIQUID NITROGEN

B/A = 6.6 f = 2.6 GHz

λ = 0.33 μm $1/\alpha$ = 11 μm

$I(W/cm^2)$	M	L	Γ	Excess Attenuation *
10	0.0006	19 μm	0.5	0 dB
100	0.0020	6.1 μm	1.8	0.9 dB
1000	0.0064	1.9 μm	5.8	5 dB
10,000	0.020	0.61 μm	18	14 dB
100,000	0.064	0.19 μm	58	23 dB

*Calculated for propagation over path much longer than L .

As seen in Table 5-1, the discontinuity lengths in water and nitrogen for 1000 W/cm^2 at 2.6 GHz are 14 μm and 3 μm, respectively. In the absence of attenuation, nonlinear effects become significant for propagation paths on the order of these lengths.

Attenuation has the effect of counteracting the formation of shock waves in the liquid. The nonlinear distortion of the wave is equivalent to the generation of higher harmonics. Since attenuation in most liquids increases as ω^2, the higher harmonics will be attenuated more rapidly than the fundamental. This tends to restore the waveform to its original sinusoidal form. Nonlinear effects in lossy liquids become important when the discontinuity length is smaller than the attenuation length. This is parameterized by Γ, the Gol'berg number

$$\Gamma = 1/\alpha L \quad .$$

Nonlinear effects are important for $\Gamma > 1$. Some representative values of the Gol'berg number are given in Table 5-1.

It is found experimentally that the fundamental frequency component of a high amplitude wave suffers greater attenuation than does a low amplitude wave. Blackstock[8] has examined in detail the phenomenon of nonlinear excess attenuation of the fundamental for plane waves. The nonlinear attenuation is due to the depletion of energy in the fundamental by the generation of harmonics. For propagation of plane waves over distances much greater than L, the excess attenuation is determined solely by Γ. In particular, Blackstock showed that for long propagation paths the excess attenuation is approximately given by

$$EXDB = -20 \log_{10}\left[\frac{4I_1(\Gamma/2)}{\Gamma I_0(\Gamma/2)}\right] ,$$

where EXDB is the nonlinear excess attenuation in decibels. The functions I_0 and I_1 are Bessel functions of imaginary argument. For $\Gamma = 1$, the excess attenuation is 0.27 dB. For $\Gamma = 10$, it is 8.9 dB.

One conclusion to be drawn from plane wave analysis is that less intensity is required in liquid nitrogen than in water for nonlinear effects to be important. For example, at 2.6 GHz the power required for $\Gamma = 1$ is 910 W/cm^2 in water and 31 W/cm^2 in liquid nitrogen.

The nonlinear propagation of plane waves is well understood. The propagation of focused beams, however, has not been as thoroughly investigated. The principle work on this subject has been done by Beyer,[7] Muir,[9] Naugol'nykh et. al.,[10] Bakhvalov et al.,[11] and Sutin,[12] among others. In addition to these acoustic studies, work done on nonlinear generation in focused optical beams is relevant. The work by Kleinman, Ashkin, and Boyd[13] on second harmonic generation in gaussian optical beams is found to be particularly useful.

B.3 The Nonlinear Wave Equation

So far we have given a general discussion describing the propagation of finite amplitude plane waves. In this section we present the mathematical basis for solving more complicated nonlinear wave propagation problems.

The equations of nonlinear acoustics have been derived by various investigators.[4,10,14] A recent work by Tjøtta and Tjøtta[4] derives the nonlinear wave equation from the Navier-Stokes equations and makes

logical connection with equations derived by others. The relationship of equations by Westervelt,[14] Blackstock,[8] Kuznetsov,[15] and Zabolotskaya and Khokhlov[16] is discussed. Most of the analysis in this chapter will be based on the equation

$$\left(\nabla^2 - \frac{1}{C_o^2}\frac{\partial^2}{\partial t^2}\right)\rho = -\frac{D}{C_o^4}\frac{\partial^3 \rho}{\partial t^3} - \frac{\beta}{\rho_o C_o^2}\frac{\partial^2}{\partial t^2}(\rho - \rho_o)^2 \tag{5.9}$$

where, as before, $\beta \equiv (1 + B/2A)$. This equation was derived by Tjøtta and Tjøtta and is similar to that used by Westervelt.[14] The first term on the right side of (5.9) is the attenuation term. The second term on the right side is the nonlinear term and leads to nonlinear distortion of the waveform and harmonic generation.

In order to find a solution to (5.9) we must specify the boundary condition

$$\rho(x,y,z,t)\Big|_{\substack{x,y,z \text{ on} \\ \text{surface } S}}$$

For the acoustic microscope the surface S of the boundary condition is the spherical lens-liquid interface. The amplitude and phase of the acoustic source at this surface is determined by the pupil function of the lens.

Before solving (5.9) in various approximations, we first examine the experimental evidence and note the features that we would like the theory to be able to explain.

C. EXPERIMENTAL RESULTS

This section describes the experimental results of operating the acoustic microscope at high power levels. In particular, the phenomena of resolution improvement and excess attenuation of the fundamental are carefully examined.

Resolution improvement through the use of high intensity focused beams was discovered when attempting to image a resolution test object in liquid argon. The test object consisted of an etched glass grating with a periodicity of 2000 Å. The acoustic lens used in this and following experiments was the 18 μm radius lens described in Chapter 4. Its performance is optimum at 2.6 GHz, though good images can be taken from 2.0 to 2.8 GHz. Figure 5-1 shows images recorded by the acoustic microscope operating at 2.0 GHz with a corresponding wavelength of 0.43 μm in the argon. At low power levels, as shown in Fig. 5-1(a), the grating is invisible and only defects on the surface are seen. When the power level is increased by 8 dB, the grating lines become faintly visible. Another 6 dB increase in transmitted power results in the grating becoming clearly resolved, as shown in Fig. 5-1(b). The sharpness of the defects also increases, indicating an overall improvement in the point response of the microscope.

It was also observed that operating the microscope at high input power levels results in an increase of microscope insertion loss. Microscope insertion loss as used here is the ratio of received power to

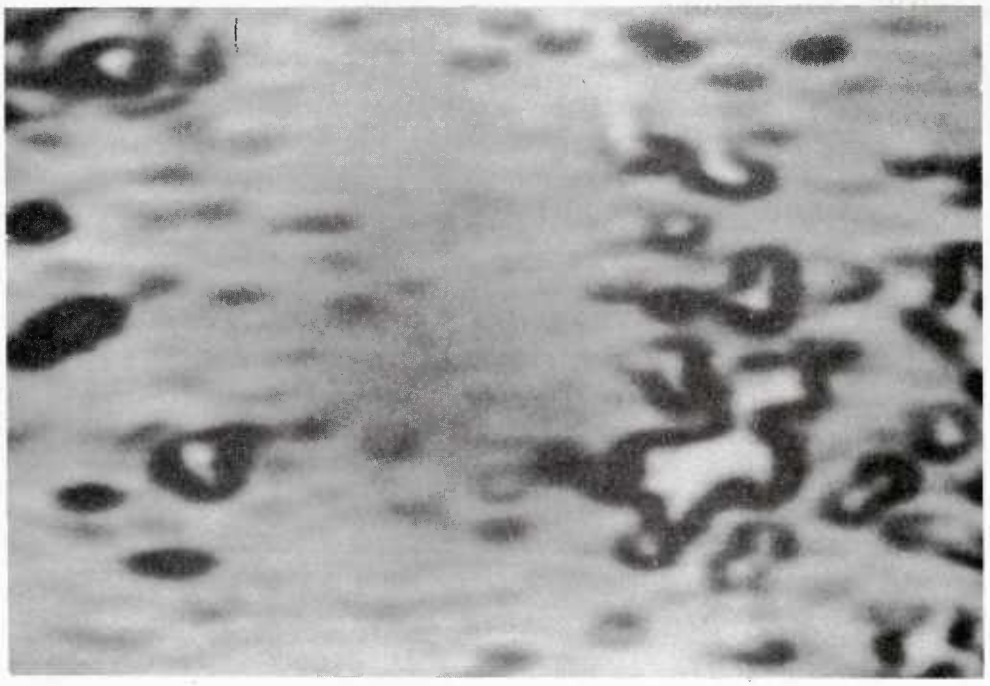

(a)

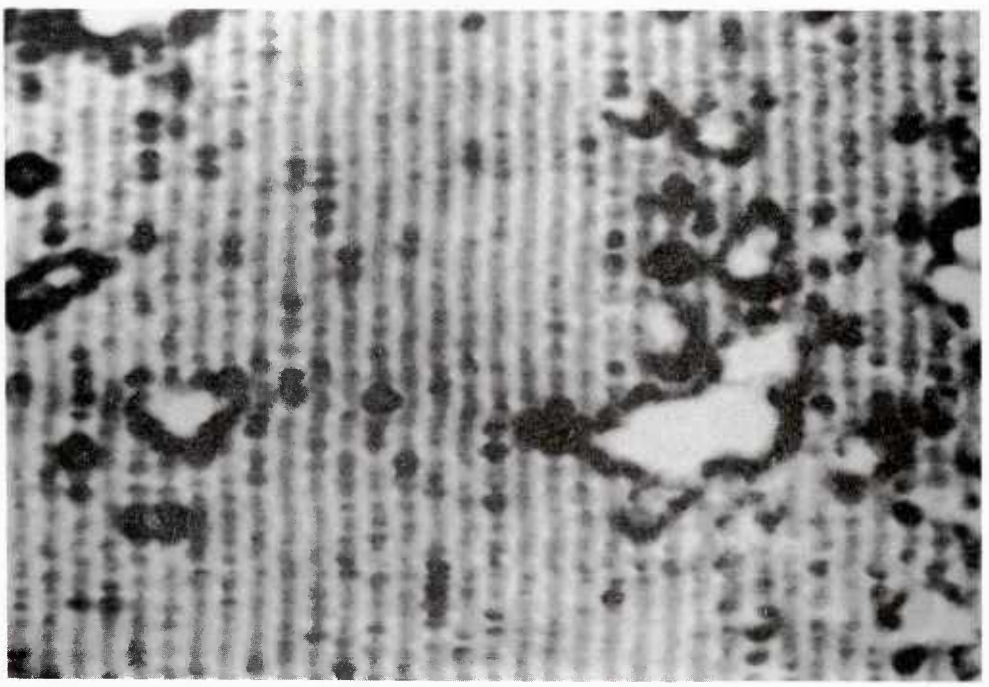

(b)

FIGURE 5.1--Nonlinear resolution of 2000 Å grating in liquid argon. Image (a) was taken at low input power, while (b) was taken at higher power.

transmitted power as measured at the electrical port of the acoustic lens. The insertion loss includes electrical mismatch loss, transducer conversion loss, lens illumination loss, acoustic lens-liquid mismatch loss, etc., as well as acoustic liquid path losses. By monitoring the reflection from the front surface of the lens, it was determined that the increase in microscope insertion loss as a function of increasing input power was the result of an effective increase in liquid path attenuation. The transducer showed insignificant nonlinear behavior. The observed excess liquid path attenuation is interpreted as resulting from depletion of the fundamental wave due to the generation of harmonics. It is similar in principle to excess attenuation observed in the propagation of plane waves, as discussed in Section B.2.

Insertion loss versus lens input power was carefully measured in liquid nitrogen and in water. The absolute lens input power was calibrated using a Hewlett-Packard Model 436A RF power meter. With this instrument the absolute power into the lens can be measured with an uncertainty of less than 5%. A Midwest Microwave Model 1044-4 step attenuator with accuracy of better than $\pm$ 0.5 dB was used to systematically step through a range of input power levels. The received power level was determined by using a Hewlett-Packard Model 393A variable attenuator placed just before the IF amplifier in the receive amplifier chain. After calibration, the received power level could be determined to within $\pm$ 0.5 dB by adjusting the receive attenuator so that the detected RF pulse height was equal to some reference voltage.

Figure 5-2 shows insertion loss vs lens input power for the acoustic lens operating at 2.0 GHz in liquid nitrogen. The object located at the focus is a silicon wafer and is assumed to be a perfect

reflector. The small solid points are the experimental data. The solid line is a smooth fit to the data points. The large solid points marked "a" - "d" are reference points which will be referred to later.

The insertion loss shown in Fig. 5-2 is seen to have the constant value of 72 dB for input power less than 10 mW. Above 10 mW the insertion loss begins to increase. The increased insertion loss results from depletion of the fundamental wave due to the generation of harmonics. Above 100 mW the insertion loss increases linearly with a slope such that a 10 dB increase in input power results in a 10 dB increase of insertion loss. Thus in the high power limit we see a saturation effect where no increase in received power is observed when transmitted power is increased.

It is useful to estimate the power and intensity at the focus for the onset of the nonlinear behavior. The lens input power level is 20 mW or 13 dBm for an excess attenuation of 1 dB. If the reflecting object located at the focus is a perfect reflector, the power level at the focus will be given by the lens input power diminished by one-half of the two-way insertion loss. Thus, for 1 dB excess attenuation the power at the focus will be -23 dBm or $P = 5 \times 10^{-6}$ W. This power is indicated by the arrow in Fig. 5-2. The peak intensity at the focus can be estimated as follows. The 1/e point of the amplitude profile occurs at a radius of approximately $w_0 = 0.55\ \lambda_0 = 0.24\ \mu m$. If the main lobe of the focus profile is approximated by a gaussian, then the intensity at the center of the focal spot is given by

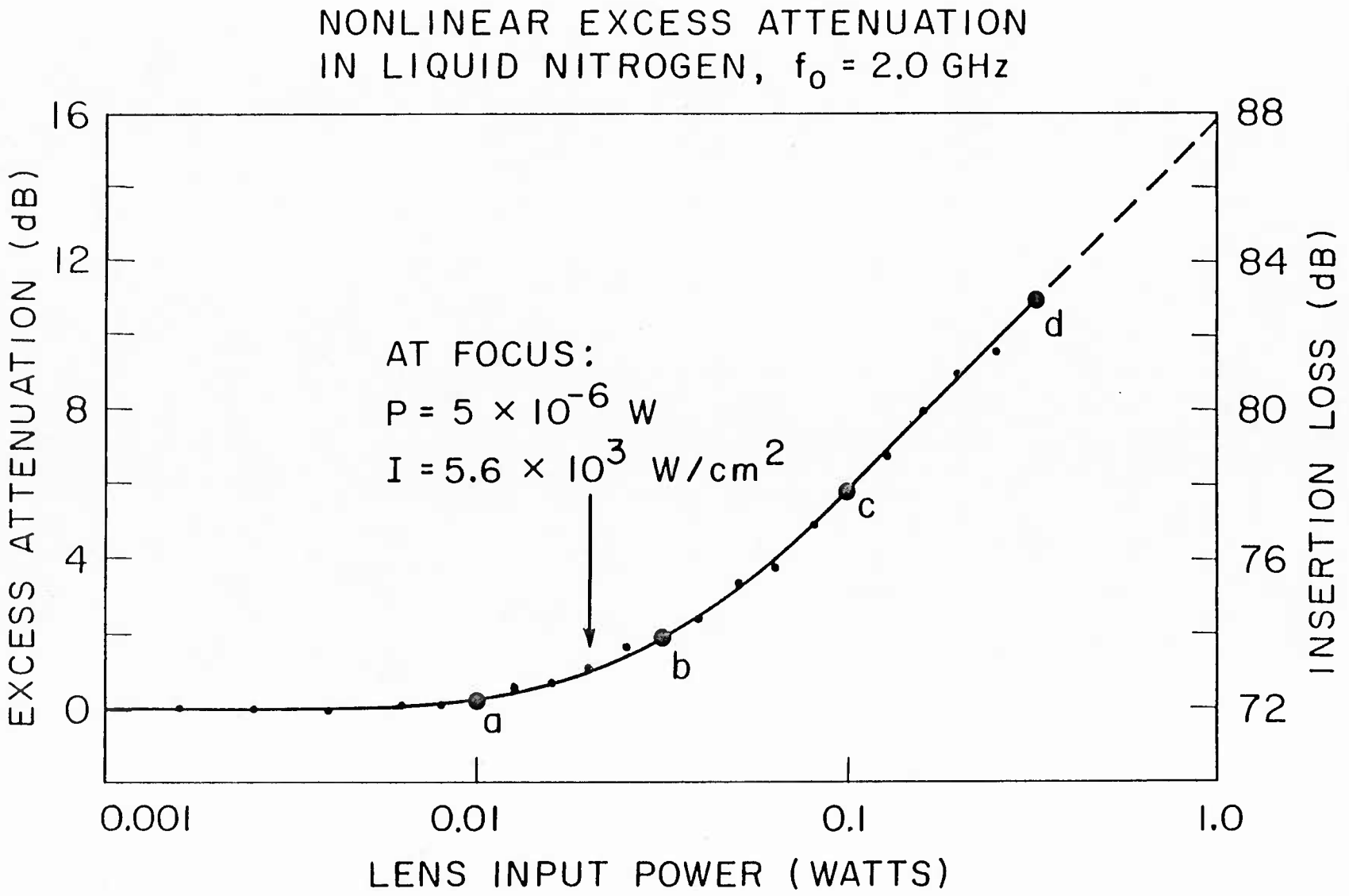

FIGURE 5.2-- Nonlinear excess attenuation in liquid nitrogen at 2.0 GHz. The solid line is a smooth curve through the experimental points. The large points are referred to in the text.

$$I = \frac{P}{(\pi w_o^2/2)} = \frac{5 \times 10^{-6}\ W}{9 \times 10^{-10} cm^2} = 5.6 \times 10^3\ W/cm^2$$

As power to the lens is increased and the excess attenuation increases, it is found that the imaging performance of the microscope improves. This effect is shown in Fig. 5-3. The object is a 0.29 μm period grating fabricated with gold lines on a silicon substrate.[18] The gold lines are approximately 400 Å wide and 500 Å thick. The input power levels at the electrical port of the acoustic lens are: (a) 10 mW, (b) 32 mW, (c) 100 mW, and (d) 320 mW. These power levels correspond to the large dots marked "a" - "d" in Fig. 5-2. The corresponding values of excess attenuation are: (a) 0 dB, (b) 2 dB, (c) 6 dB, and (d) 11 dB. The signal-to-noise ratio in the images was kept approximately constant by insertion of attenuators at the receive port of the circulator.

The grating pattern is not visible in Figs. 5-3(a) or (b). This is because the periodicity of the grating is so small that its spatial frequency is beyond the spatial frequency cutoff of the microscope when operating linearly (low power). Increasing the input power 5 dB beyond that used in Fig. 5-3(b) causes the grating to become clearly visible, as can be seen in Fig. 5-3(c). This is evidence that the spatial frequency response of the microscope has been extended by use of the higher power. Increasing the input power another 5 dB further improves the grating contrast, as shown in Fig. 5-3(d).

Thus we have demonstrated that resolution improves when the microscope is operated in the nonlinear regime. We now estimate the

NONLINEAR RESOLUTION OF 0.29μm GRATING IN LIQUID NITROGEN
f_0 = 2.0 GHz, λ_0 = 0.43 μm

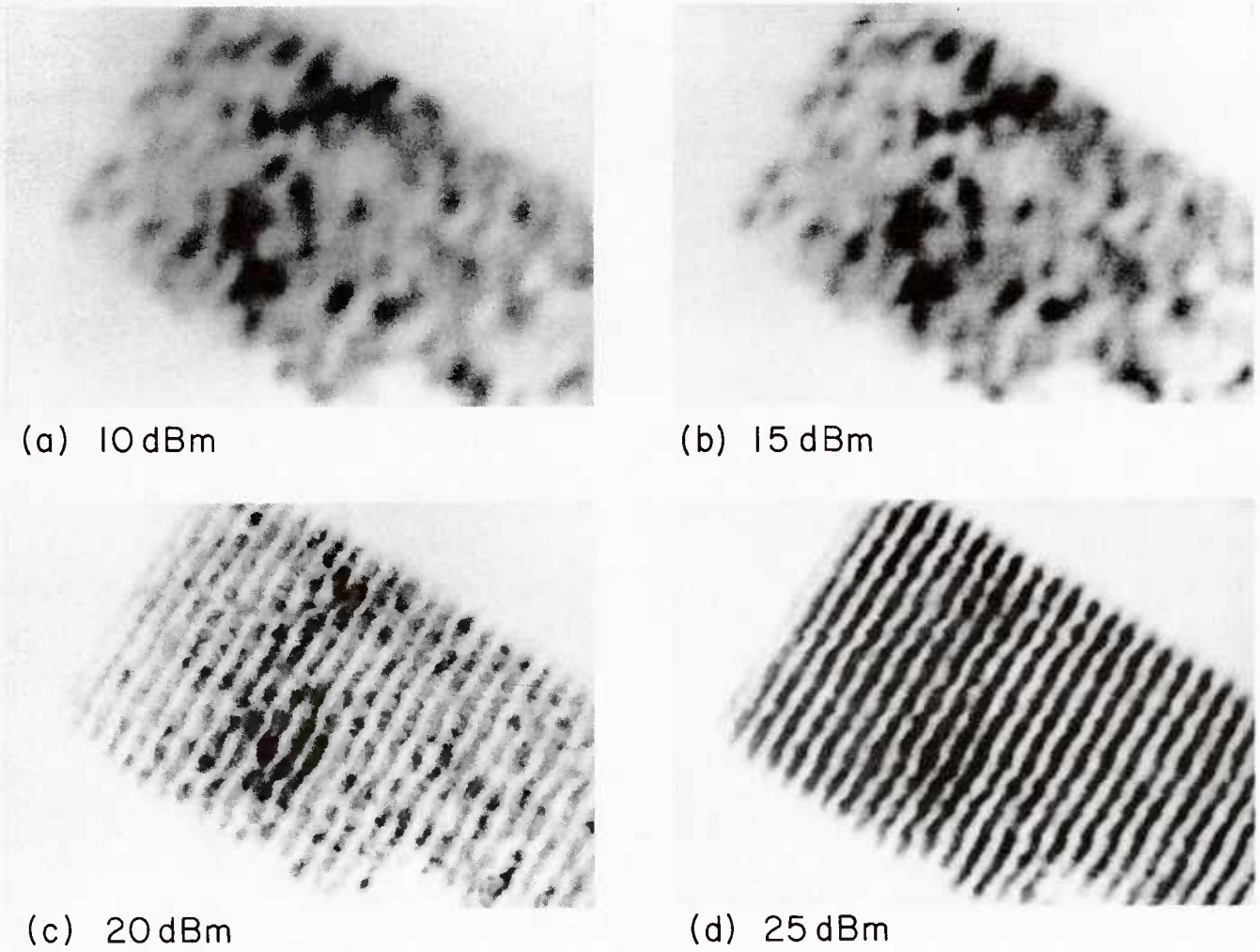

(a) 10 dBm (b) 15 dBm

(c) 20 dBm (d) 25 dBm

FIGURE 5.3--Demonstration of resolution improvement as a function of lens input power.

amount of resolution improvement. Figure 5-4 shows another set of images taken in liquid nitrogen. The object is a gold-on-silicon grating similar to the previous grating. The periodicity, however, is reduced to 0.21 μm. In Fig. 5-4(a) we see that the grating is not resolved when imaged at 2.0 GHz in the linear regime. If the power is increased so that the imaging is nonlinear, the grating is clearly resolved [Fig. 5-4(b)]. If the frequency is increased to 2.8 GHz and linear imaging is used, the image in Fig. 5-4(c) results. It is unclear whether the grating is resolved in this image. It is obvious, however, that the image exhibits poorer resolution than that of image (b). In Fig. 5-4(d), nonlinear imaging at 2.8 GHz is used and the grating is seen with excellent contrast.

A lower bound for resolution improvement can now be set. Linear imaging at 2.8 GHz [Fig. 5-4(c)] will have resolution approximately 1.4 times better than that of linear imaging at 2.0 GHz [Fig. 5-4(a)]. This follows from the decrease in wavelength which results from the increase in frequency. Since nonlinear imaging at 2.0 GHz [Fig. 5-4(b)] shows better resolution than linear imaging at 2.8 GHz [Fig. 5-4(c)], it follows that by operating the microscope in the nonlinear regime the resolution of the imaging improves by at least a factor of 1.4.

The factor of 1.4 increase in resolution is a significant improvement. To understand how significant it is, one must consider the alternative means of improving resolution. If the opening angle of the lens is fixed, the only way to improve resolution (apart from using a different liquid medium) is to increase the operating frequency of the lens. However, this is not easily accomplished, since the liquid attenuation in decibels increases as the square of the operating

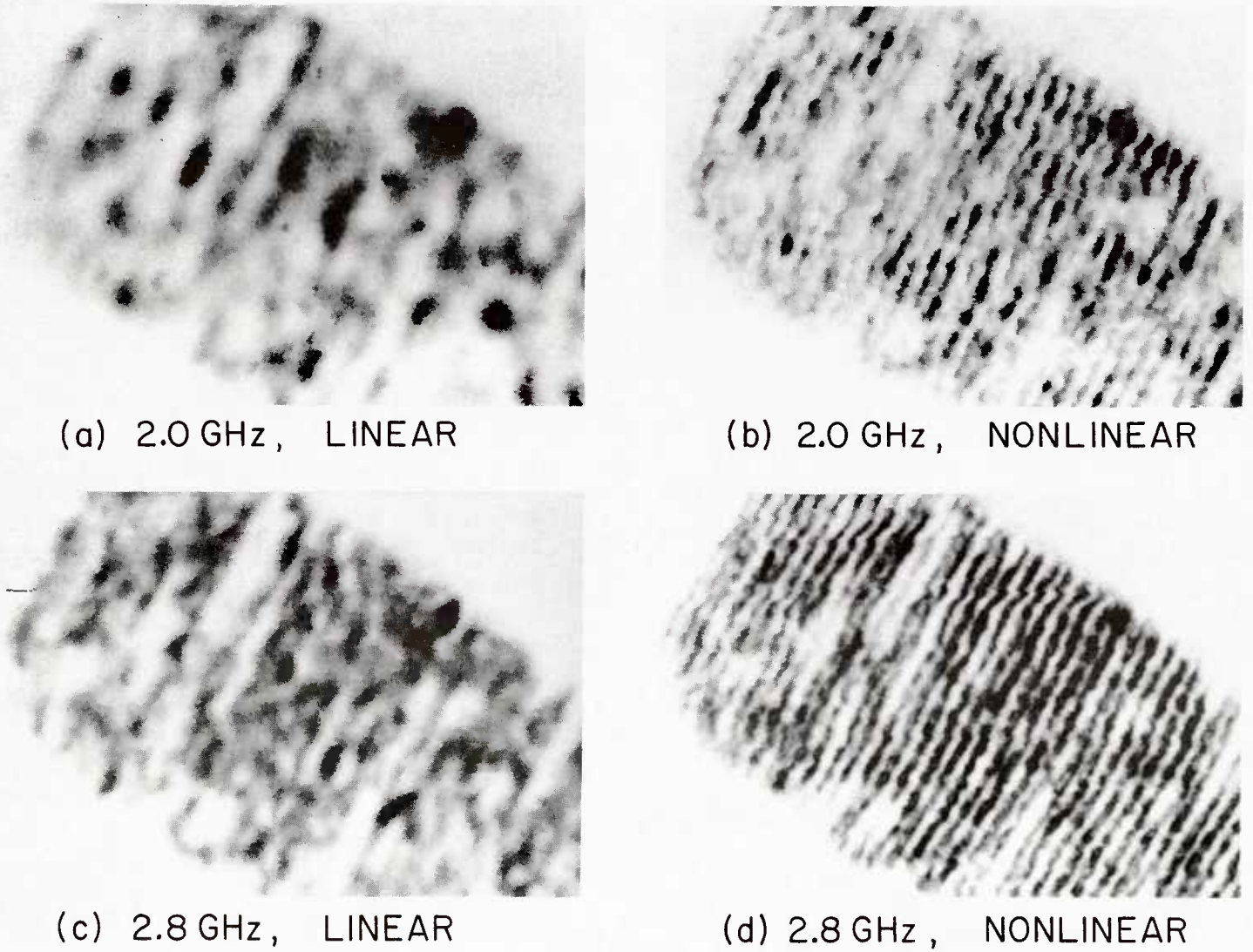

FIGURE 5.4--Nonlinear resolution of 0.21 μm grating in liquid nitrogen. From these images a lower bound on amount of resolution improvement can be set (see text).

frequency. Thus, to offset the increase in attenuation accompanying a 1.4 increase in frequency, the liquid path and, therefore, the lens radius must be halved. This is the approach that was taken by Jipson[19] to improve microscope resolution. There is, however, a limit to how small the lens radius can be made and still be practical for imaging objects with several microns of surface topography. Since the lens radius we are using in this study is only 18 μm, a halving of the radius to 9 μm would reduce the working space to what is perhaps an impractical level.

Nonlinear resolution improvement and excess attenuation have been observed in water as well as in cryogenic fluids. Figure 5-5 shows excess attenuation vs lens input power at 2.6 GHz for the same lens operating in either liquid nitrogen or water at 60°C. For a lens input power less than 1 mW, both liquids are operating in the linear regime. The onset of nonlinear behavior occurs at approximately 3 mW for liquid nitrogen and 60 mW for water. For nitrogen the power at the focus corresponding to the onset of nonlinearity is $P = 1.3 \times 10^{-6} W$. In water the required power is higher: $P = 1.3 \times 10^{-4} W$. The intensity at the focus can be estimated as it was done for Fig. 5-2. The focal spot size in nitrogen is $w_o = 0.55 \lambda = 0.18$ μm . The intensity for onset of nonlinearity is, therefore, $2.6 \times 10^3 W/cm^2$. In water the spot size is somewhat larger due to the longer wavelength, $w_o = 0.32$ μm , and the intensity at the focus for the onset of nonlinearity is $8.1 \times 10^4 W/cm^2$.

The above results show that, in comparison to nitrogen, greater power levels are necessary for the acoustic propagation through water to be nonlinear. In light of the results presented in Section B, this

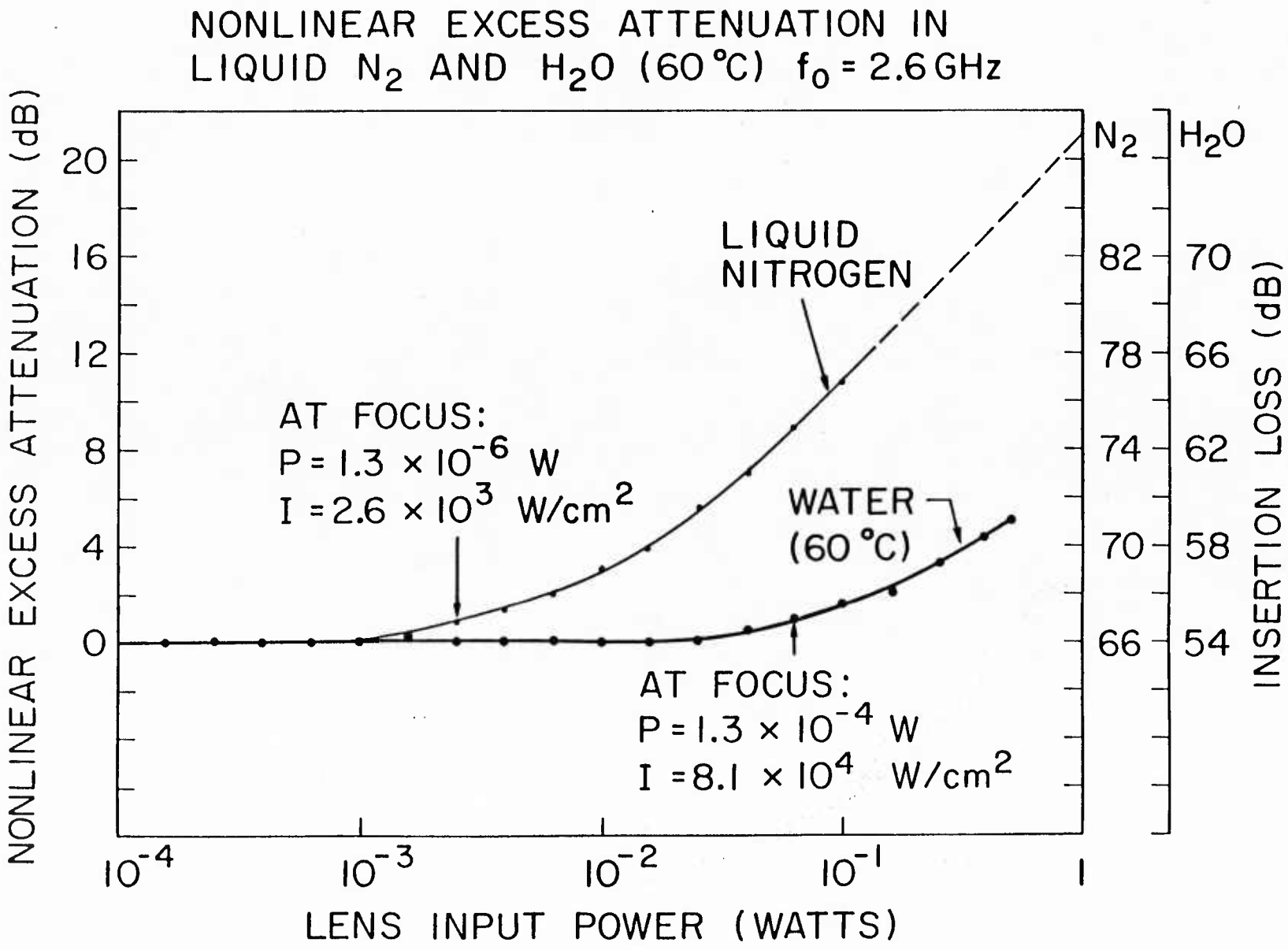

FIGURE 5.5--Comparison of measured nonlinear excess attenuation in liquid nitrogen and water.

result is not surprising as it was shown that, for equal power levels, the Gol'berg number is significantly smaller in water than in nitrogen.

When operating at or near the power level required for saturation, it is possible to observe nonlinear resolution improvement in hot water. Figure 5-6 shows an image of a 0.3 μm grating taken in 60°C water at 2.6 GHz with a lens input power of approximately 2 W. The grating structure can be clearly seen in the image. This image is probably the highest resolution image that has ever been taken by acoustic microscopy in water. The grating was not visible at low input power.

D. PHYSICAL MODEL FOR NONLINEAR RESOLUTION IMPROVEMENT

In the previous section it was demonstrated that the resolution of the acoustic microscope increases for high input power. In this section we present a simple physical model which accounts for this effect in a qualitative way.

It is well documented that high intensity acoustic beams generate harmonics and that the harmonic beams exhibit smaller angular spread than the fundamental.[9] In the case of focused beams we would expect the focused spot size of the harmonic beams to be smaller than the spot size of the fundamental beam. This has been shown to be true for optical beams.[13] Thus if we were transmitting at the fundamental frequency (ω_1) and receiving the second harmonic ($2\omega_1$), we would expect to see improved imaging resolution. What we wish to explain here is why the increased resolution is seen when receiving the fundamental frequency.

Figure 5-7 shows a schematic diagram of wave propagation in the focused beam. To make the diagram less confusing we consider a

NONLINEAR RESOLUTION OF 0.3 μm GRATING IN WATER (60 °C)

$f_0 = 2.6$ GHz, $\lambda_0 = 0.58\,\mu$m

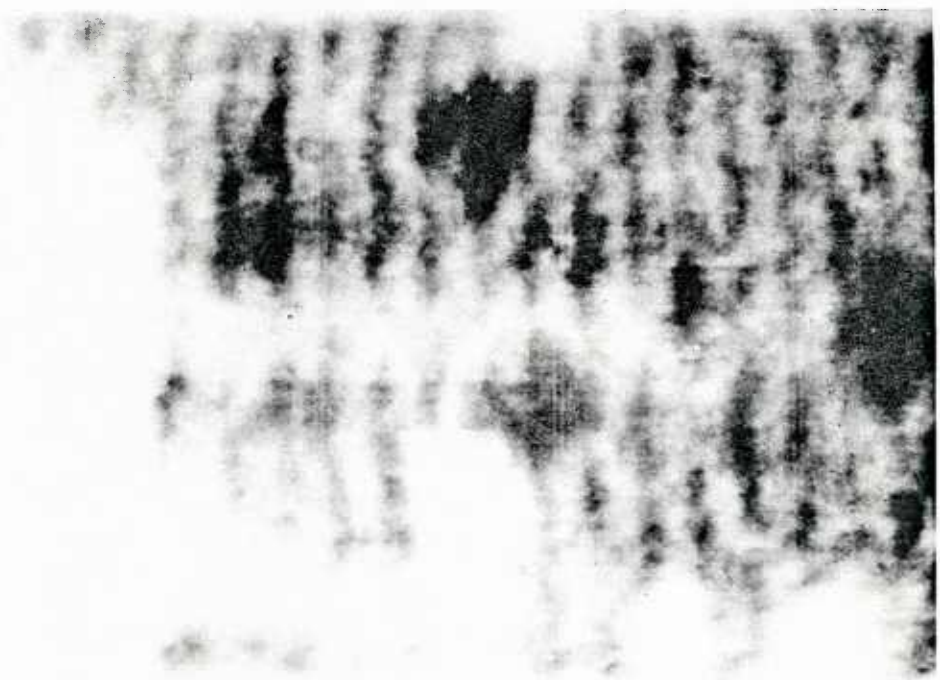

FIGURE 5.6--Nonlinear resolution of 0.3 μm grating in water at 2.6 GHz.

FIGURE 5.7

SIMPLE THEORY OF RESOLUTION IMPROVEMENT

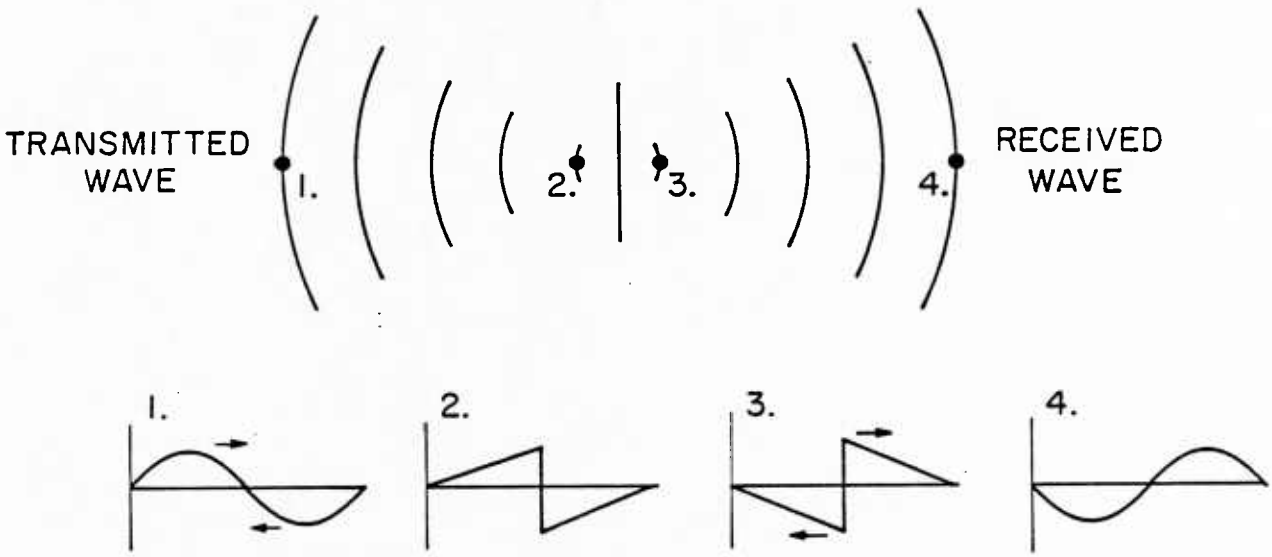

1. Incoming wave is initially sinusoidal.
2. Peak travels faster than trough due to nonlinearity; harmonics are generated near the focus. Harmonics focus to smaller diffraction limited spot than fundamental.
3. Passage through focus results in π phase shift of all harmonics. Peak now lags.
4. Peak moves forward, feeding energy of harmonics into fundamental and restoring sinusoidal waveform.

transmission example rather than reflection. The two cases are equivalent if the reflector is perfectly rigid. Because of the lack of phase matching, the nonlinear interaction of waves propagating in opposite directions is negligible.

At point 1 in the diagram an initially sinusoidal wave is launched into the liquid. The intensity of the wave increases as it propagates due to geometrical focusing of the beam. As the wave propagates, the pressure peak travels faster than the trough and the waveform is distorted into the shape of a sawtooth wave. The distortion of the wave into the sawtooth shape is equivalent to the generation of harmonics. These harmonics will focus to a smaller diffraction-limited spot size in the focal plane than will the fundamental because of the shorter wavelength associated with the harmonics. The smaller spot size associated with the harmonics is responsible for the increase in resolution. Passage through the focal region results in an overall π phase shift of all harmonic components. This phase shift is a well known property of focused beams.[20] After the π phase shift, the waveform will look like that shown at point 3 in the diagram. This sawtooth has a lagging pressure peak and a leading pressure trough. As it propagates, the peak will advance in the waveform and the trough will be retarded. This results in a net decrease in the distortion of the wave and is equivalent to the feeding of energy from the harmonics back into the fundamental. Thus we have a mechanism for communicating the high resolution information contained on the generated harmonics back to the fundamental frequency.

REFERENCES FOR SECTION 5

1. R. Kompfner and R.A. Lemons, Appl. Phys. Lett. 28, 295 (1976); R.A. Lemons, Ph.D. Dissertation, Stanford University (1975).
2. C. Yeack, M. Chodorow, and C.C. Cutler, J. Appl. Phys. 51, 4631 (1980); C. Yeack, Ph.D. Dissertation, Stanford University (1980).
3. L.D. Landau and E.M. Lifshitz, Fluid Mechanics (Pergamon, Oxford, (1959).
4. J.N. Tjøtta and S. Tjøtta, J. Acoust. Soc. Am. 69, 1644 (1981).
5. R.D. Fay, J. Acoust. Soc. Am. 3, 222 (1931).
6. O.V. Rudenko and S.I. Soluyan, Theoretical Foundations of Nonlinear Acoustics (Plenum, New York, 1977).
7. R.T. Beyer, Nonlinear Acoustics (Naval Sea Systems Command, Dept. of the Navy, 1974), Chapter 3.
8. D.T. Blackstock, J. Acoust. Soc. Am. 36, 534 (1964).
9. T.G. Muir, in Acoustical Imaging (Plenum, New York, 1981), Vol. 9, p. 93.
10. K.A. Naugol'nykh, S.I. Soluyan, and R.V. Khokhlov, Sov. Phys. Acoust. 9, 42 (1963).
11. N.S. Bakhvalov, Y.M. Zhileikin, E.A. Zabolotskaya, and R.V. Khokhlov, Sov. Phys. Acoust. 24, 10 (1978).
12. A.M. Sutin, Sov. Phys. Acoust. 24, 334 (1978).
13. D.A. Kleinman, A. Ashkin, and G.D. Boyd, Phys. Rev. 145, 338 (1966).
14. P.J. Westervelt, J. Acoust. Soc. Am. 35, 535 (1963).
15. V.P. Kuznetsov, Sov. Phys. Acoust. 16, 467 (1971).

16. E.A. Zabolotskaya and R.V. Khokhlov, Sov. Phys. Acoust. 15, 35 (1969).

17. F. Ingenito and A.O. Williams, J. Acoust. Soc. Am. 49, 319 (1971).

18. Courtesy of R. Howard, Bell Telephone Labs.

19. V. Jipson and C.F. Quate, Appl. Phys. Lett. 32, 789 (1978).

20. M. Born and E. Wolf, Principles of Optics (Pergamon, Oxford, 1980), pp. 447-448.

ACTIVITIES DURING THE PERIOD OF CONTRACT

Awards

D. Rugar	-	1981-82 F. V. Hunt Fellowship in Acoustics, Acoustical Society of America
C. F. Quate	-	1981 IEEE Morris N. Liebmann Award "For development of an acoustic microscope capable of sub-micron resolution"
C. F. Quate	-	1982 Rank Prize for Opto-Electronics "In recognition of contribution to medical, biological and physical research through the concept of the scanning acoustic microscope, which uses sound rather than light to form images."

Invited Talks/Meetings

"Ultrasonic Imaging", Rank Prize Funds International Symposium on "Electronic Imaging," September 13, 1978, Royal Society, London, England (C. F. Quate)

"The Scanning Acoustic Microscope", Optical Society of America, November 1, 1978, San Francisco, California (C. F. Quate)

"Acoustic Microscopy at Cryogenic Temperatures", 96th Meeting of the Acoustical Society of America, 27 November-1 December, 1978, Honolulu, Hawaii. J. Acoust. Soc. Am. 64, Suppl. 1, S62, 1978 (J. Heiserman and D. Rugar)

"The Mechanically Scanned Acoustic Microscope", American Physical Society, March 19, 1979, Chicago, Illinois (C. F. Quate)

Kompfner Lecture Series, Bell Laboratories, Holmdel, New Jersey, May 14, 1979. Abstract entitled "Acoustic Microscopy" (C. F. Quate)

"New Results in Ultrasonic Microscopy", 50th Anniversary Meeting, Acoustical Society of America, June 13, 1979, Cambridge, Massachusetts (C. F. Quate)

Max-Planck-Institut fur Festkorperforschung, Stuttgart, West Germany, December 10, 1979. Talk entitled "Acoustic Microscopy at Microwave Frequencies" (C. F. Quate)

University of California, Santa Cruz, Department of Natural Science, California, April 3, 1980. Talk entitled "A New Form of Microscopy with Acoustic Waves" (C. F. Quate)

"Cryogenic Acoustic Microscopy", Rank Prize Funds International Symposium on "Scanned Image Microscopy", September 22-24, 1980, Royal Society, London, England (J. Heiserman)

"Microwaves, Acoustics and Scanning Microscopy", Rank Prize Funds International Symposium on "Scanned Image Microscopy", September 22-24, 1980, Royal Society, London, England (C. F. Quate)

Invited Talks/Meetings, continued

"Acoustic Microscopy at Optical Wavelengths", 100th Meeting of the Acoustical Society of America, 17-21 November, 1980, Los Angeles, California, J. Acoust. Soc. Am. 68, Suppl. 1, B1 (J. Heiserman)

Princeton University, Department of Physics, February 26, 1981. Abstract entitled "The Acoustic Microscope - a System for Imaging with Microwaves" (C. F. Quate)

College of Engineering, University of Colorado, Boulder, March 12, 1981. Abstract entitled "The Acoustic Microscope - a System for Imaging with Microwaves" (C. F. Quate)

"Microscopy and Imaging with Acoustics and Photoacoustics", Laser '81 Opto-Elektronik Conference, 5th International Congress and International Trade Fair, June 4, 1981, Munich, West Germany (C. F. Quate)

Chevron Oil Field Research Company, La Habra, California, June 16, 1981. Talk entitled "The Acoustic Microscope: a Fundamentally New Instrument for Obtaining Images and Characterizing Materials at the Microscopic Level" (C. F. Quate)

"Cryogenic Acoustic Microscopy: the Search for Ultrahigh Resolution using Cryogenic Liquids", Sixteenth International Conference on Low Temperature Physics (LT-16), August 19-26, 1981, University of California at Los Angeles, California (J. Heiserman)

"Resolution Improvement in the Acoustic Microscope using High Intensity Focused Beams", 1981 IEEE Ultrasonics Symposium, October 14-16, 1981, Chicago, Illinois (D. Rugar)

"Acoustic and Photoacoustic Microscopy in the Study of the Elastic Properties of Surfaces", Surface Science Symposium with the People's Republic of China, sponsored by Xerox Palo Alto Research Center, October 20, 1981, Palo Alto, California (C. F. Quate)

"Acoustic Microscopy", Naval Postgraduate School, Monterey, California, October 23, 1981 (C. F. Quate)

"Theory of Resolution Improvement in a Focused Acoustic Imaging System using High Intensities", 103rd Meeting of the Acoustical Society of America, April 26-30, 1982, Chicago, Illinois, J. Acoust. Soc. Am. 71, Suppl. 1, S30 (D. Rugar)

Oxford University, Department of Electrical Science, Oxford, England, April 29, 1982. Talk entitled "Imaging with Scanning and Acoustics" (C. F. Quate)

University of California, Davis, Department of Physics, June 1, 1982. Talk entitled "Acoustic Imaging and Microscopy" (C. F. Quate)

104th Meeting of the Acoustical Society of America, Orlando, Florida, November 8-12, 1982. Paper entitled "Acoustic Microscopy" (C. F. Quate)

Santa Clara Chapter of IEEE Sonics and Ultrasonics, January 1983. Talk entitled "Ultrahigh Resolution in the Acoustic Microscope" (D. Rugar)

Invited Talks/Meetings, continued

Golden Gate Metals and Welding Conference, San Francisco, California, February 9-11, 1983. Talk entitled "Microscopy via Acoustics and Photoacoustics" (C. F. Quate)

Third International Topical Meeting on Photoacoustic and Photothermal Spectroscopy, Paris, France, April 5-8, 1983 (C. F. Quate, Chairman of Session on "Thermal Waves and Non-Destructive Control")

Fourth International Conference on Phonon Scattering in Condensed Matter, Stuttgart, West Germany, August 22-26, 1983. Paper entitled "Two Applications of Microwave Acoustics in Liquid Helium: High Resolution Microscopy and Direct Measurement of Phonon Dispersion" (D. Rugar)

1983 IEEE Ultrasonics Symposium, Atlanta, Georgia, October 31-November 2, 1983. Paper entitled "Recent Developments in High Resolution Acoustic Microscopy at Stanford" (D. Rugar)

106th Meeting of the Acoustical Society of America, San Diego, California, November 8-11, 1983. Paper entitled "New Applications of Nonlinear Acoustics at Microwave Frequencies", Special Session on Novel Application of Macrosonics, (D. Rugar)

American Physical Society Meeting, Detroit, Michigan, March 26-30, 1984. Talk entitled "Thermal Phonon Detection in Superfluid Helium using the Acoustic Microscope" (J. S. Foster)

Publications

C. F. Quate, "Ultrasonic Imaging", in Electronic Imaging, Rank Prize Funds International Symposium, London, England, September 1978, P. Schagen and T. McLean, Eds. (Academic Press Ltd, 1979), pp. 365-393.

J. Heiserman, D. Rugar and C. F. Quate, "Cryogenic Acoustic Microscopy", J. Acoust. Soc. Am. 67, 1629-1637 (May 1980).

C. F. Quate, "Microwaves, Acoustics and Scanning Microscopy", in Scanned Image Microscopy, Rank Prize Funds International Symposium, London, England, September 1980, E. A. Ash, Ed. (Academic Press Ltd, 1980), pp. 23-55.

J. Heiserman, "Cryogenic Acoustic Microscopy", in Scanned Image Microscopy, Rank Prize Funds International Symposium, London, England, September 1980, E. A. Ash, Ed. (Academic Press Ltd, 1980), pp. 71-96.

D. Rugar, J. Heiserman, S. Minden and C. F. Quate, "Acoustic Microscopy of Human Metaphase Chromosomes", J. of Microscopy, 120, 193-199 (November 1980).

C. F. Quate, "The Acoustic Microscope: a Concept of Microscopy using Waves of Sound", Naval Research Reviews, Office of Naval Research, Vol. XXXIII, No. 1, 24-32 (Fall-Winter 1980-81).

J. Heiserman, "Acoustic Measurements in Superfluid Helium", Section 8 in Methods of Experimental Physics, Vol. 19 (Ultrasonics), P. Edmonds, Ed. (Academic Press, 1981), pp. 413-453.

Publications, continued

C. F. Quate, 1981 Science Year, Annual Supplement of the World Book Encyclopedia. Photograph supplied of chick embryo fibroblasts comparing optical and acoustic images.

J. Heiserman, "Cryogenic Acoustic Microscopy: the Search for Ultrahigh Resolution using Cryogenic Liquids", Physica, 109 & 110B, 1978-89 (North-Holland Publishing Company, 1982).

J. Heiserman, "Thermal Grounding of a Transmission Line in a Dilution Refrigerator", Cryogenics, 243-44 (May 1982).

D. Rugar, J. S. Foster and J. Heiserman, "Acoustic Microscopy at Temperatures Less than 0.2°K", in Acoustical Imaging, Vol. 12, E. A. Ash and C. R. Hill, Eds. (Plenum Press, New York, 1982), pp. 13-25.

J. S. Foster and D. Rugar, "High Resolution Acoustic Microscopy in Superfluid Helium", Appl. Phys. Lett. 42, 869-71 (15 May 1983).

D. Rugar, "Two Applications of Microwave Acoustics in Liquid Helium: High Resolution Microscopy and Direct Measurement of Phonon Dispersion", in Phonon Scattering in Condensed Matter, Proceedings of the Fourth International Conference on Phonon Scattering in Condensed Matter, Vol. 51, W. Eisenmenger, K. Labmann and S. Döttinger, Eds. (Springer-Verlag, Berlin, 1984), pp. 26-33.

D. Rugar, "Resolution Beyond the Diffraction Limit in the Acoustic Microscope: A Nonlinear Effect", J. Appl. Phys. 56, 1338-46 (1 September 1984).

D. Rugar and J. S. Foster, "Accurate Measurement of Low-Energy Phonon Dispersion in Liquid ^{4}He", Phys. Rev. B, 30, 2595-2602 (1 September 1984).

B. Hadimioglu and J. S. Foster, "Advances in Superfluid Helium Acoustic Microscopy", J. Appl. Phys. 56, 1976-80 (1 October 1984).

Manuscripts

J. Foster, "High Resolution Acoustic Microscopy in Superfluid Helium", presented at 17th International Conference on Low Temperature Physics, Karlsruhe, West Germany, August 15-22, 1984. To be published in Physica, January 1985.

J. S. Foster and D. Rugar, "Low Temperature Acoustic Microscopy", to be published in Special Issue of IEEE Transactions on Sonics and Ultrasonics, 1985.

B. Hadimioglu and J. S. Foster, "Recent Developments in Superfluid Helium Acoustic Microscopy", presented at the 1984 IEEE Ultrasonics Symposium, November 14-16, Dallas, Texas. To be published in the Proceedings of the Ultrasonics Symposium.

J. S. Foster and S. Putterman, "Parametric Self-Enhancement of the Spontaneous Decay of Sound in Superfluid Helium", to be submitted to Physical Review Letters.

Reports

Semiannual Report, 1 July 1977-1 January 1978 (G.L. Report No. 2773)

Annual Report, 1 July 1977-30 June 1978 (G.L. Report No. 2865) (AD A060391)

Semiannual Report, 1 July 1978-1 January 1979 (G.L. Report No. 2921)

Annual Report, 1 July 1978-30 June 1979 (G.L. Report No. 3008) (AD A074502)

Semiannual Report, 1 July 1979-1 January 1980 (G.L. Report No. 3083)

Annual Report, 1 July 1979-30 June 1980 (G.L. Report No. 3149) (AD A087677)

Semiannual Report, 1 July 1980-1 January 1981 (G.L. Report No. 3241)

Annual Report, 1 July 1980-30 June 1981 (G.L. Report No. 3369) (AD 109271)

Semiannual Report, 1 January 1981-1 July 1981 (G.L. Report No. 3336)

Semiannual Report, 1 July 1981-1 January 1982 (G.L. Report No. 3388)

Summary Report, July 1977-June 1982 (G.L. No. 3435)

Annual Report, 1 July 1981-30 June 1982 (G.L. No. 3481) (AD A119705)

Semiannual Report, 1 July 1982-1 January 1983 (G.L. No. 3541)

Annual Report, 1 July 1982-30 June 1983 (G.L. Report No. 3628) (AD A135089)

Personnel

C. F. Quate	--	Principal Investigator
J. Heiserman	--	Research Associate - entered Medical School, Stanford University Medical Center, September 1981
D. Rugar	--	Research Associate - Ph.D. Thesis entitled: "Cryogenic Acoustic Microscopy", Stanford University, December 1981. Accepted position at IBM Research Laboratory, San Jose, California, May 1984.
J. S. Foster	--	Research Associate - Ph.D. Thesis entitled: "Superfluid Helium Acoustic Microscopy", Stanford University, June 1984. Appointed Chodorow Fellow in Applied Physics, Stanford University, September 1984.